SANDIA REPORT
SAND2018-8608
Unlimited Release
Printed Month and Year

HERMES Outdoor Shot Series 10268-313: Data Analysis as a Model for Output Voltage and Current Estimates for HERMES Shots; a User Perspective

Timothy J. Renk

Prepared by
Sandia National Laboratories
Albuquerque, New Mexico 87185 and Livermore, California 94550

Sandia National Laboratories is a multimission laboratory managed and operated by National Technology and Engineering Solutions of Sandia, LLC, a wholly owned subsidiary of Honeywell International, Inc., for the U.S. Department of Energy's National Nuclear Security Administration under contract DE-NA0003525.

Issued by Sandia National Laboratories, operated for the United States Department of Energy by National Technology and Engineering Solutions of Sandia, LLC.

Available to DOE and DOE contractors from

U.S. Department of Energy
Office of Scientific and Technical Information
P.O. Box 62
Oak Ridge, TN 37831

Telephone: (865) 576-8401
Facsimile: (865) 576-5728
E-Mail: reports@osti.gov
Online ordering: http://www.osti.gov/scitech

Available to the public from

U.S. Department of Commerce
National Technical Information Service
5301 Shawnee Rd
Alexandria, VA 22312

Telephone: (800) 553-6847
Facsimile: (703) 605-6900
E-Mail: orders@ntis.gov
Online order: https://classic.ntis.gov/help/order-methods/

SAND2018-8608
Printed August 2018
Unlimited Release

HERMES Outdoor Shot Series 10268-313: Data Analysis as a Model for Output Voltage and Current Estimates for HERMES Shots; a User Perspective

Timothy J. Renk
Directed Energy Assessments
Sandia National Laboratories
P. O. Box 5800
Albuquerque, New Mexico 87185-MS1182

Abstract

The primary subject of this Report is the description and characterization of results (voltages, currents, radiation dose and dose-rates) from the HERMES accelerator operated in the Outdoor Mode. The shots described range from 10266 – 10313, and were taken in late 2016. In the course of determining the most accurate estimates of voltage and current, a prescriptive procedure is developed to process the raw data posted to the HERMES database. The current estimates are tied to voltage determination using the MITL theory of Mendel, as modified by Schumer and Ottinger. The converter currents are accurately recorded due to newly calibrated monitors at the converter location. Additional historical information about the development of the HERMES current monitor set is included to enhance the archival value of this Report. The evolution of the TLD faceplate profile from non-peaked center to center-peaked is discussed, with hypotheses as to the cause. The prescriptive procedure discussed herein is accurate as of the day of printing. Should the prescription be modified and updated, this Report would also need updating.

ACKNOWLEDGMENTS

The author acknowledges fruitful conversations concerning this Report with Dr. Keith Cartwright, the Principal Investigator for the Outdoor test series described here, who provided the funding for writing the manuscript, and who also reviewed the manuscript. The author acknowledges the important contribution of Dr. Paul Ottinger, formerly of the Naval Research Laboratory (retired) and currently with Syntek Technologies in Arlington, VA. Dr. Ottinger provided updated LSP simulations extending the results of earlier work, detailed in a 2006 paper (Ottinger and Schumer). The updated results are discussed starting on page 43 of this Report. Two key advances beyond the 2006 work are: a) extension of the MITL voltage from 10 to 20 MV, and b) use of the actual HERMES load region geometry, instead of the generic load discussed in the 2006 work. The author also acknowledges the contribution of Dr. Bruce Weber of the Naval Research Laboratory, who devised the alternative dose-area weighting procedure I have adopted to analyze the 29 faceplate TLDs. The procedure, described in Appendix 1, is set up within an Excel spreadsheet, and uses the 'Trapezoidal Rule' to process the 29 TLDs. This method is an alternative to the 'TLDsum' recorded for each HERMES shots, which adds up the dose from each of the 29 TLDs. And finally, the author acknowledges the contribution of Russell Durrer (1342), who performed the MCNP simulations that demonstrate that the HERMES electron beam does not pinch to the radius of the graphite plug during the main radiation pulse (Appendix 1).

TABLE OF CONTENTS

FIGURES

EXECUTIVE SUMMARY

1. The major HERMES monitor signals (IAS, MK7, PINB, SCD) used in the data analysis for this Report are described, along with some of the history of their origin and development. These details form a useful addition to the HERMES knowledge base for both staff and users. In particular, it should be noted that for this Report, the IAS4 and IAS5 current monitors (close to the converter) *have been calibrated for the first time*. This allows for a more accurate estimate of the current reaching the Outdoor Mode converter. Initial calibrations for IAS4 and IAS5 were obtained during the July 2017 Ion Diode test series (Shot 10458). A more accurate determination was obtained from the half-machine short-circuit shot (10634) executed as part of the April 2018 Ion Diode test series. Those calibrations will be used here.

2. A PRESCRIPTIVE PROCEDURE is developed for processing HERMES data, starting from the H3xxxxxcc.HDF files in the HERMES database, and leading to final estimates of currents and voltages for the Outdoor Mode shots (10368-10313) that are the subject of this Report. In the process, a number of assumptions and judgement calls as to the required data processing (e.g. de-drooping, gauge factor adjustments, selective monitor exclusions) are clearly stated, and caveats given. These assumptions/judgement calls are the sole responsibility of the author, and are taken with the dataset as it is known in the latter half of 2017. In the event of future changes to data interpretation, updates to this Report will be appropriate and necessary.

3. In view of the lack of an absolute calibration of HERMES output voltage, considerable effort is taken to connect the HERMES data to the major theory of MITL operation, that of Mendel as modified by Ottinger and Schumer (NRL 2006). The result of that effort is a plausible positioning of the HERMES total-bound currents (and derived load voltages) in the extrapolated voltage contours in Z_oI_c-Z_oI_a space. While the derived estimate of ~ 18-18.5 MV and ~ 650 kA for, respectively, load voltage and current for a full-power bremsstrahlung HERMES shot appear plausible, and consistent with previous efforts to estimate these parameters (e.g. Sanford 2013), enough remaining uncertainties (monitor calibration, variability in monitor output among the typical 4 monitors making up any averaged (AVE) signal, and uncertainties in the 'g' factor) exist to limit the accuracy of these parameters to ~ ±1 MV and ~ 30-50 kA, in the view of the author. In particular, the 'g' factor scales with the electron emission threshold at the cathode, because this affects the current profile of the flow as a function of distance from the center conductor. While a 150-250 kV/cm threshold is generally accepted by the pulsed power community, this factor is unknown for HERMES fielding conditions, but can be estimated at ~ 370 kV/cm.

4. In the process of analyzing these and other HERMES data, useful additions to the HERMES dataset have been developed. In particular,
    1. Looking over the last ~ 1000 HERMES shots, it appears that there has been a slight but perceptible increase in the power coming forward. Load voltages have increased an estimated ~ 0.5 to 1 MV over this time period. This is ascribable to the extensive efforts by Gary Tilley and his fielding team to optimize HERMES cavity and Marx performance.
    2. One possible side-effect of this increase in forward-going power is the increased tendency of the HERMES electron beam to pinch, leading to damage on the converter

package. This could be due to the increased current striking the converter and liberating an increased amount of surface monolayers and entrained gasses on the converter. This could lead to increased ion inventory, resulting in an enhanced pinch to the axis. One mitigation is to increase the A-K gap. This does not affect the load impedance, since the diode operates at self-limited conditions, but the electron orbits *are* affected, specifically spread outward from the diode axis so as to decrease the probability of the electrons pinching.

3. Estimates of current to the Outdoor Mode converter have been refined, since for the first time, the IAS4 monitors at the converter have been calibrated.

5. Evidence is presented that the dose-rate monitors (SCD and PINB) can be of help in describing the dynamics of the electron beam operation during the HERMES power pulse. At present, however, the benefit is largely qualitative, not quantitative. This would change if the monitors could have accompanying TLDs fielded on each shot, so the dose could be absolutely calibrated. A significant additional benefit would result from a full ITS-CYLTRAN modeling of the dose-rate monitors in the HERMES load region.

NOMENCLATURE

[On odd-numbered page]

Abbreviation	Definition
Abbreviation	Definition
MITL	Magnetically insulated transmission line
TLD	Thermoluminescent dosimeter
LSP	Particle-in-cell code, software product of ATK Mission Research, Albuquerque, NM.
MCNP	Monte Carlo N-Particle Transport Code, software package developed by Los Alamos National Laboratory

2. INTRODUCTION

This report describes the characterization of voltage and current transport in experiments designed to deliver photon dose to the HERMES facility outdoor 'courtyard' in support of validation experiments. The HERMES accelerator (18 MV, 650 kA, 40 ns) uses an Inductive Voltage Adder (IVA) architecture to deliver current through a Magnetically Insulated Transmission Line (MITL) to a Bremsstrahlung electron diode. The concept of such a diode connected to an MITL can be described by referring to the conceptual drawing below (Figure 1), taken from a previous Sandia Report (T.W.L. Sanford, History of HERMES III Diode to Z-Pinch Breakthrough and Beyond, SAND2013-2481, April 2013). The HERMES IVA lies to the left. The MITL consists of two parallel cylinders, one centered inside the other, with the inner cylinder cantilevered within the outer. The outer radius of the inner conductor (cathode in negative polarity) and inner radius of the outer cylinder dimensions are 18.5 cm and 32.6 cm, respectively. As the power pulse delivered by HERMES progresses from left to right, the normal electric field at the cathode exceeds the threshold for electron emission. If the MITL is operating correctly, after an initial loss front, the electron current becomes magnetically insulated, and propagates along and close to the inner conductor. This electron current is referred to as *flow*, and is schematically depicted in the Figure as two curved lines that follow the inner conductor for a short time, then diverge slightly in the anode-cathode (A-K) gap (marked as e-). The flow in HERMES experiments is quite large. For example, in a typical full-power HERMES shot, out of 650 kA, about 2/3 of this current consists of flow current. The ~ 200 kA remainder flows within the inner conductor as *bound* current, which is then emitted in the A-K gap and added to the flow current. The flow is depicted at three different points in the power pulse: early in time (A), when current is lost to the outer conductor, midway through the rise (or fall – B), when the current flows ~parallel to the two conductors, and at peak power (C), when the flow converges towards the converter. At the converter, electrons strike a Tantalum foil, emitting Bremsstrahlung photons which at these energies are concentrated in the 'forward' (right) direction. A set of thermoluminescent dosimeters (TLDs) is arrayed in a radial pattern attached to the outside of the vacuum plate that is at the right of the converter. This is known as the 'Faceplate TLD array' and will be explained in detail later in this Report.

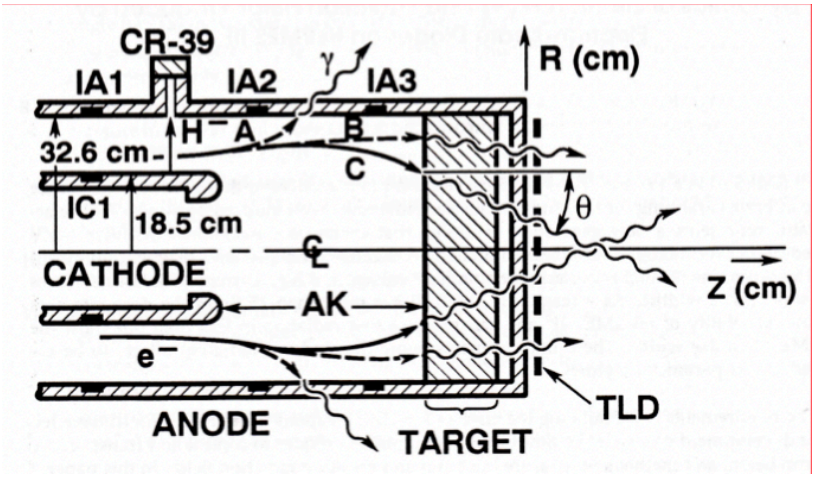

Figure 1. HERMES III Extended Planar-Anode diode illustrating electron trajectories and radiation produced at (A) early or late time, (B) midway through the voltage rise or fall, and (C) peak power. AK gap > 50 cm.

The hardware design depicted in the Figure above is referred to as the Standard Mode. The 18.5 cm and 32.6 cm radii of the inner and outer MITLs results in large diameter hardware. For any number of experiments, particularly with diagnostics and test objects located in the external 'Courtyard', it is desirable to extend the MITL to the edge of the interior 'Test Cell' so that the converter is located approximately at the boundary of the Test Cell and the Courtyard at the rollup door position. Previous experiments indicate that the most photon dose to locations in the Courtyard is achieved by extending the MITL length to a converter location as close to the door as possible, rather than by keeping the converter at the Standard Mode position. This is due to the fall-off in photon intensity as the distance squared. But since this is a distance of some 11 meters, and since the inner MITL conductor is cantilevered, it has long been considered impossible to continue these large conductor dimensions the entire 11 meter length. This is because the additional cantilevered weight has been estimated to put excessive mechanical strain back at the connection point to the HERMES cells. [As of this writing, a new 11 meter MITL design is planned to keep the large inner and outer MITL dimensions, by the use of very thin conductor material.] And so an alternative MITL structure was designed.

The original attempt to extend the MITL hardware to the rollup door consisted of keeping the outer hardware, and simply eliminating the center conductor. The entire volume is then filled with air at some low pressure, a concept known as a 'gas cell'. Despite some level of success at current transport, the lack of a center conductor significantly limited net current transport to the door location. The decision was made to return to a center conductor, but one with significant weight reduction compared to the large diameter inner conductor making up the Standard Mode. An extension was added to the inner conductor that begins with the 18.5 cm OD indicated above, but then tapers linearly down to 4.44 cm radius (3.5 inch diameter) over a length of 4 meters. It then continues at fixed radius for another 0.89 meters. This length of inner conductor then constitutes the cathode for the Extended Mode, which is not discussed here. This ~ 5 meter extension is still well short of the ~ 11 meters needed for the MITL hardware to reach the position of the rollup door. An additional length of 3.5 inch-diameter MITL is added to span the remaining distance. This extension is made from sheet aluminum approximately 35 mils in thickness, with no internal support structure, this to save weight. This design cannot remain level over this distance, and develops a natural 'droop' of ~ 3.5 degrees. This 'droop' has a beneficial side-effect. Since the floor of the Test Cell is ~ 9 feet above the courtyard floor, the droop actually results in increased directed photon illumination of test objects mounted in the Courtyard. A detrimental side-effect of the small diameter and weight-savings requirement is that there are no bound (inner) current monitors built into the long inner MITL extension.

The outer MITL must then be drooped in an equivalent manner. This accomplished by inserting a 'swivel-flange that is longer on top than at the bottom. Additional sections are then added to match the length of the inner conductor. Figure 2 below depicts a schematic side-view of the outer conductor in place. This configuration is referred to as the 'Outdoor Mode'.

The position marked 'IAS1' at the right refers to the location of the upstream total current monitors. The location of the Standard Mode converter is approximately two meters to the left of the IAS1 position. The converter for the Outdoor Mode is located at the far left. The (4) IAS1 current monitors measure the total current at the (right) input end of the MITL. Near their position are (4) monitors called MK7 located on the inner MITL, which measure the bound current at the input end.

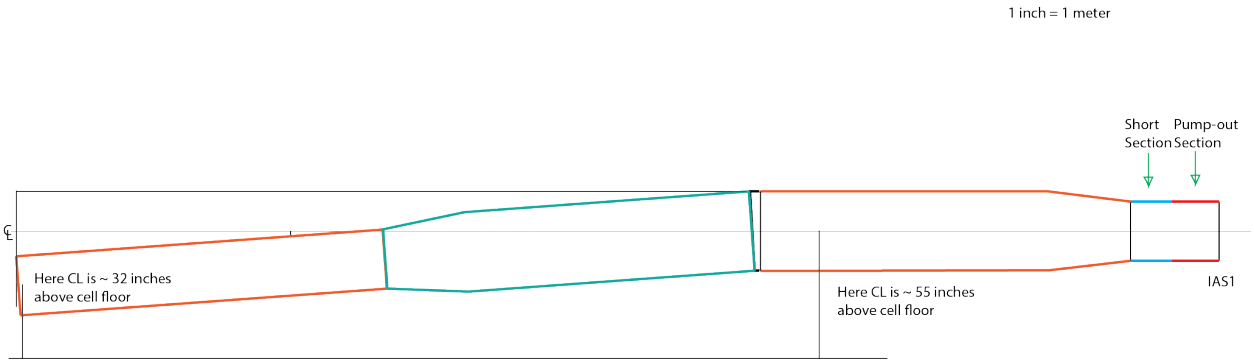

Figure 2. Schematic diagram depicting the (outer) MITL in the Outdoor Mode.

The panoramic photograph below depicts the Outdoor Mode outer conductor in place:

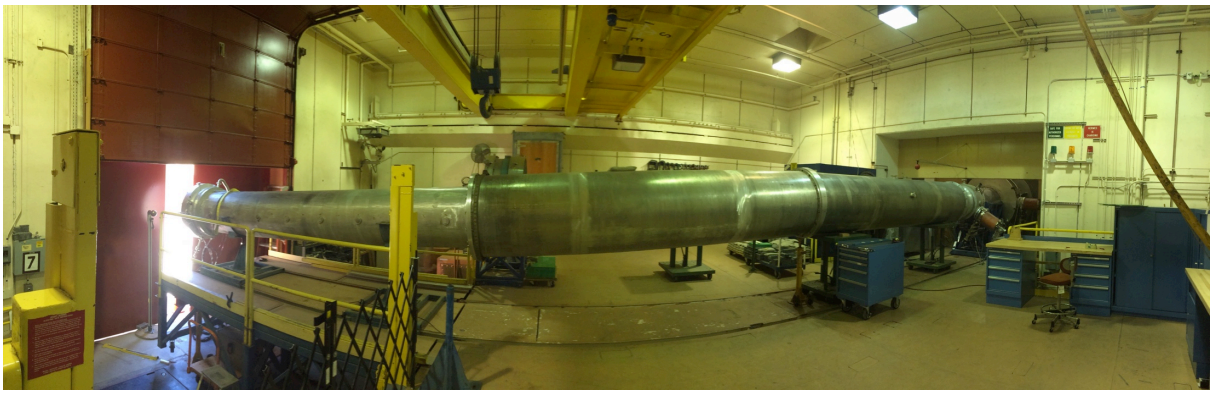

Figure 3. Photograph of the outer MITL in place in the Outdoor Mode.

While the use of this inner-outer conductor pair results in significantly more current reaching the conductor than is the case with the gas cell, considerable current loss still exists with this mode. There are several reasons for this: 1) tapering the inner conductor to 3.5 inches diameter increases the MITL vacuum impedance from 34 to 119 ohms. Such an impedance mismatch results in significant expected loss of MITL flow, since at the higher impedance, less current is carried in flow under equilibrium conditions; 2) at the same time, the outer conductor ID is *increased*, from 25.5 inches to 34.25 inches, further raising the MITL impedance in this section to 137 ohms. The use of larger-diameter parts occurred because such parts were on-hand at the time of construction; 3) The 34.25-inch section (middle of the photograph above) transitions back to 25.5 inches (left side of photograph), again due to use of parts on-hand. Thus, because a) the change in MITL impedance is so large, b) the length of impedance change is so long, and c) there is a transition out and back in from the 137-ohm section, the net result is a loss of more than half the input current at the converter, compared to the input measured at the IAS1 position. In addition, the 3.5° bend apparently results in preferential electron loss to the top of the MITL, confirmed by TLDs placed along the MITL. This expected top-bottom asymmetry in current flow is also reflected in a slight but systematic shift in the centroid of the faceplate TLDs above the center-line (far left in the photograph). As for the IAS4 monitors, while they are situated within 5 cm of the converter, there are only two monitor locations, located horizontally across from each other at the 090 and 270 positions (with 0° at the top). Thus, no top-bottom current comparisons are available. (Data from the two 090 and 270 monitors indicates some amount of east-west asymmetry in current flow on some shots.)

Further discussion of the hardware setup and simulation results can be found in the report titled 'Coupled EM-PIC/Rad-Transport Simulations of HERMES Courtyard Experiments', by Tim Pointon *et al*.

This Report has three goals:

1) **quantification of the current loss associated with the Outdoor Mode MITL hardware, e.g. level of current measured at IAS4 compared to the input current at IAS1.** This includes characterization of the dose behavior at the converter as indicated by the faceplate TLDs. The courtyard TLD arrays are not included in this discussion. Dose-rate characterization is also investigated, using the P-I-N detector (PINB) mounted on the left-hand Test Cell wall (visible at extreme-left in the photograph), and two spherical Compton diodes, SCD and SCDREF. The SCD monitor is mounted on a movable stand, and positioned near the converter at a roughly 45° angle. The SCDREF monitor is hung from a boom so as to be in front of the converter at the Standard Mode position (the boom is barely visible at the far-right of the photograph). In the Outdoor Mode, SCDREF is ~ 11 meters away from the converter, and its line-of sight is blocked by the MITL itself. Consequently, it is of marginal utility for Outdoor Mode shots. As will be seen, SCD data can be well-correlated to the faceplate TLD data, and provides some insight into electron dynamics at the converter position. The PINB data is also useful, although less so than the SCD data.

2) **Precise quantification of HERMES output voltage and current.** This entails two prerequisites: a) accurate values for current at various positions in both the inner and outer MITLs. For monitors co-located at the same z-location on both inner and outer MITLS (e.g. MK7 and IAS1), voltage at that location can be calculated using the Mendel theory and variations (see References). The Mendel theory is discussed more extensively below; and b) translation of current and diagnostic data recorded by the HERMES Data Acquisition System (DAS) into final form as best estimates of such currents. At present, the raw data recorded by DAS are *not* in this final form. Consequently, a major goal of this Report is to present a prescription for arriving at the data in final form, starting from the raw HERMES data as posted after a given shot on the STL website. The path taken to this final form is the one devised by the author of this Report. In this writeup, the various decisions made about how this path is given are listed in detailed form, taking into account historical developments in the HERMES database. Conclusions are then developed about the behavior of the Outdoor Shots that are the main subject of this Report.

3) **Document the performance of HERMES during this shot series.** It is hoped that by determining, for example, more precise values for forward-going current and voltage on HERMES, that this document will be of archival use to both HERMES staff and HERMES users. There is a fair amount of information here – the history of the MK7 cathode monitors, for example – that is outside the current Org. 1342 corporate memory. A such, this report should be considered as a modern-day extension of a previous document (Reference 1), a 'Guide for Users' published as a Sandia Report in 1989 by Gerry Zawadzkas. This 48-page earlier document provides considerable useful information about the HERMES facility. Much of the information is relevant today – Isodose maps for HERMES shots, for example, - while other portions of the Report – Computer resources, for example, are out-of-date. In addition, another Sandia Report (Reference 2), a 116-page document published by Tom Sanford in 2013, gives extensive historical and technical information about the development of HERMES III as a gamma-radiation facility.

Determining 'true' current: caveats. The principal method of determining accurate values of current in pulsed power hardware is to execute a *short-circuit* shot. Such a shot is performed by connecting anode and cathode with metal so that no voltage difference between them can occur. Since the inner and outer conductors move closer as to each other as the vacuum system evacuates the air, the metal connection must be flexible. (On HERMES, in Standard Mode, the outer conductor moves approximately 7 mm closer axially towards the inner conductor as high-vacuum is attained.) In practice, aluminum foil is formed into a ball and inserted between the anode and cathode. During pump down, the 'ball' can be reduced in length and still remain a viable short. The assumption behind short-circuit current operation is that current monitors relatively close to the short-circuit load (say within 10 ns transit time) must read the same value, since no voltage difference develops during the power pulse. In this way, currents can be compared, and gauge factors can be set, *relative to each other*. But in this method, there is no procedure for determining *absolute values* for current. The latter requires a separate experiment, such as a calorimeter-based approach under development (Chris Grabowski, private conversation), the goal of which is to determine by measuring energy deposition an accurate estimate of the current flowing into the calorimeter.

In lieu of knowing absolute current values, this Report takes the position that while true voltage and current on HERMES shots cannot be absolutely determined at this time, a very good estimate can be made, using a combination of 1) Mendel theory as modified by Ottinger and Schumer (Ottinger 2006), self-consistency-of-data arguments, and consideration of voltage determination of prior researchers, such as the work of Sanford and Halbleib (Sanford 2013). Furthermore, the techniques listed below began to be used starting a number of years ago, in collaboration with Victor Harper-Slaboszewicz, and with his general agreement as to methods.

One such self-consistency argument is as follows: in the Mendel theory, and under equilibrium conditions for electron flow in a MITL, the voltage at a particular point can be derived if the total current I_a and bound current I_c are both known at that same point. The expression for the voltage V is (Ottinger 2006)

$$\mathbf{V = Z_0(I_a^2 - I_c^2)^{1/2} - [(gmc^2/2e)* (I_a^2-I_c^2)/I_c^2]} \qquad \mathbf{(1)}$$

where Z_0 is the vacuum impedance of the MITL, and g is a parameter of order 1. (If g is set = 1, the original Mendel equation is recovered.) At HERMES parameters, the first term is by far the largest. The subtractive second term, sometimes termed the *space charge* term, amounts to ~ 5% of the total for full-power shots.

This equation leads to a set of solutions which, when plotted in Z_0I_c-Z_0I_a space, yield a set of hyperbola-like curves as depicted in Figure 4 below, again from Ottinger 2006. The HERMES bremsstrahlung diode makes use of a very large A-K gap, = 53 cm for the shots discussed in this Report. For such a large A-K gap, the diode can be said to run in the 'self-limited' mode. In the Figure 4 plot, the self- limited mode lies close to the 'minimum-current flow' line shown. For the output voltage shown, the voltage-total current values can be readily calculated using the minimum-current line. For a canonical HERMES output voltage of 18 MV, Ia = 600 kA, and for a hypothetical 20 MV, Ia = 700 kA (g=1, Tim Pointon, private conversation). With some variation, these numbers are consistent with reported values of HERMES output voltage-current as reported by previous researchers. Analogous numbers reached for the shots listed in this Report are similar to these, but there are several caveats. The first is that the value of g has been adjusted here, as per private conversations with Paul Ottinger, because in the original work by Mendel, values of output voltage as high as 18 MV were not considered. The value of g is estimated at 1.2 for this Report,

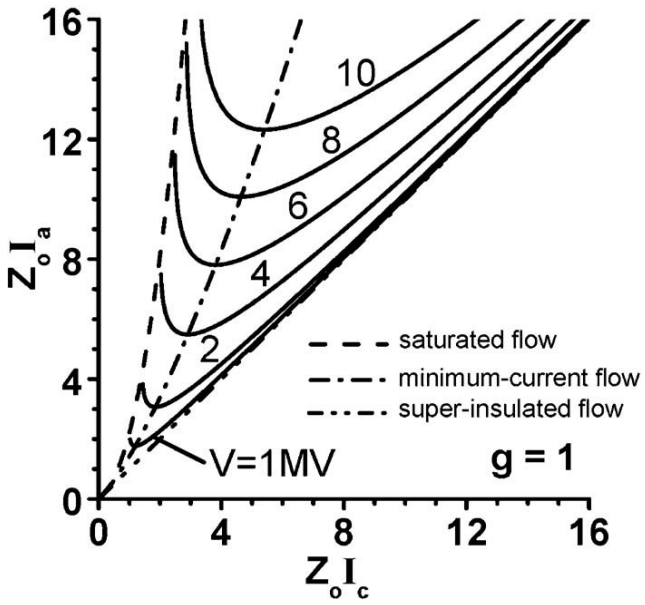

Figure 4. Plot of the anode current I_a as a function of the cathode current I_c for equilibrium MITL flow for a range of voltages. The locations of saturated flow, minimum-current flow, and super-insulated flow are plotted.

which lowers the output voltage by ~ 0.5 MV over that estimated with g = 1. The second is that in the Ottinger-Schumer paper, it is concluded that, in fact, self-limited current does NOT correspond to the minimum-current curve in the plot above, but rather to the left of it, towards the 'saturated' portion of the plot. This may further shift the relationship between V and Ia. Still, the conclusion of this Report that for the shots that are featured here, where HERMES is operating at optimal output, typical voltages at IAS1 are in the upper-18MV – lower 19 MV range, with total currents ~ 640 – 660 kA. These values are within the range discussed above.

Another caveat about deriving the voltage-current data is that the prescription section below is written for processing with the XDAMP waveform processing software. Terms such a 'dedroop' have a specific meaning and process within XDAMP and would have to be modified to fit other processing protocols such as LABVIEW.

3. PRESCRIPTION FOR DERIVING OUTPUT VOLTAGES AND CURRENTS FROM HERMES DAS DATA

After a given HERMES shot, data from that shot are stored at the STL website:

stl.sandia.gov/Data/Hermes/

Groups of 100 shots are stored together in a single folder. As of the writing of this Report, the folder 'HERMES107' is being populated with shots in the 10700-799 range. For each shot, there are a number of files stored. The relevant files for waveform analysis have a H3_xxxxx.HDF suffix, for processing within XDAMP. For example, there are two such files with the following format:

H3_10433.HDF
H3_10433cc.HDF

where the shot number is the 5-digit numeral in the middle, in this case Shot 10433. The file name marked with 'cc' (cable-compensated) will be the focus of this discussion, and the file without the 'cc' will not be used.

The shot waveforms stored in the xxx.HDF files (and some waveforms not stored in those files) must be corrected for three effects:

1. Cable-compensation
2. De-drooping
3. Signal selection for averaging, and gauge factor changes

Cable compensation is needed for all the cables which transport signals to the DAS screen room, due to changes in the waveforms caused by the long transport distance. Of the two H3_xxxxx.HDF file types listed above, the one labeled 'cc' contains cable-compensation for the waveforms stored in the file. The 'cc' file is derived from the non-'cc' file, by running a cable-compensation protocol inherited from shots pre-9800, and traceable to Joe Gergel, Jr. More recently, cable compensations have been measured again for the principal cables making up the HERMES cable plant, e.g. IAS1, IAS2, and the dose-rate monitors (PIN, SCD, SCDREF). The exact details of how cable-compensation is performed is outside the scope of this Report, but details can be obtained from HERMES DAS personnel. Comparisons between the 'old' and 'new' cable compensation routines have been performed by the author and by Victor Harper-Slaboszewicz. Differences between say the IAS1 waveforms have been found to be small, in the 1-2% range. Accordingly, for this Report, the H3_xxxxxcc.HDF files have been used as the starting point, since the cable-compensations for principle waveforms are already calculated.

'De-drooping' refers to the requirement to further process certain signals beyond the cable-compensation routine discussed above, which is required for all signals. There are two types of current monitors fielded in the HERMES MITL: Bdots and shunt current monitors. Bdots measure changes in magnetic field due to the current passing by. The signals are sent to DAS in non-time-integrated form (hence the 'dot'), and must be software-integrated. The gauge factors for Bdot waveforms are typically quite large (~ 2e11, for example). These waveforms do not require de-drooping. Important Bdot signals are the MK7 and MK6 sets of monitors, located on the inner (cathode) MITL in the vicinity of the IAS1 monitors.

Shunt current monitors, on the other hand, exhibit a RC time-constant in their decay and suffer what is known as 'droop', a modification to their waveform induced by the transport to DAS. A major symptom of

droop is a tendency of a given waveform to decrease below Zero after peak power (for positive-going signals). To correct for this, a 'deDroop' command is available within XDAMP. To select it, one chooses 'Special', then 'deDroop', and enter a value into 'Input the e-folding time'. Again, the technical details for how to execute 'dedrooping' outside of the XDAMP software are beyond the scope of this Report. Users without access to XDAMP, or are without motivation to use it, are encouraged to discuss further details with HERMES DAS personnel.

The selection of the proper e-folding time is obtained empirically, by comparison with signals from the non – dedrooped monitors located nearby. The principle shunt current monitors in need of de-drooping are the IAS1, IAS2, and IAS3 monitors, all located in the Standard Mode hardware on the outer (anode) MITL. The IAS4 and IAS5 current monitors, located within the Outdoor Mode hardware, also require dedrooping, but since these signals are not listed within the H3_xxxxxcc.HDF file, they will be discussed separately below.

For example, the monitors IAS1 and MK7 are located on the outer and inner MITLs, respectively, and are close enough in axial location to be used to calculate voltage using the Mendel protocol (Eq. 1 above). The 4 individual monitors making up each set are retrieved from the H3_xxxxxcc.HDF file, and averaged (discussed below). Then the IAS1-averaged signal is de-drooped so that the 'tail' of the waveform (i.e. after peak current) matches the post-peak MK7 'tail'. A value of **275 ns** for the IAS1 dedroop is found to match the tails of IAS1 and MK7 together, for the shots featured in this Report. This match occurs for both short-circuit and full-power HERMES shots using 275 ns. This same value is chosen for all IASxcc monitor sets, and the resultant signal tails in all cases are found to match reasonably well. It should be pointed out that the dedroop factor is found to change, especially in newer shots outside the scope of this Report, and dedroop factors as high as 400 ns have been observed by the author. Such changes in the dedroop factor have relatively minor consequences for the IAS waveform, amounting to ~ 5 – 10 kA differences in peak current.

It must be pointed out here that the dedrooping protocol discussed above, indeed the very idea that the current shunts need to be 'dedrooped', is a point of controversy. Arguments will be developed below that strengthen the argument for dedrooping the current shunts. But as with other features of this Report, the author takes responsibility for all decisions made in this Report.

Signal selection for averaging, and gauge factor changes. More Caveats and Disclaimers. The procedures outlined above about de-drooping and cable-compensation can be characterized as routine techniques. This section, however, involves data interpretation, and employs what some may term judgement calls. The rationale for the data interpretation, and the procedures that derive from it, are clearly stated in this section, and are the sole responsibility of the author. The steps described here are those taken as of the printing date of this Report. In the event that key aspects of this procedure change in the future, such changes will be detailed in a future Report. The data processing steps are detailed for, as an example HERMES shot, Shot 10433 (listed above). This is a full-power Standard Mode bremsstrahlung diode shot with a 53-cm A-K gap.

The entire list of **Data Interpretation Conclusions** is listed just below, then developed in detail in the discussion that follows:

1. **For the purposes of calculating the average IAS1 current (IAS1_AVE), for this Report, IAS1090 will be excluded.**
2. **The IAS1-3cc current waveforms will be de-drooped at a value of time constant 275 ns.**
3. **The IAS1-3 monitor calibrations in place since 2011 will be retained.**
4. **The MK7 monitor calibrations in place since Shot 9680 will remain unchanged.**
5. **For this Report, The MK7 average peak value will be assumed to be in the 200-300 kA range.**

6. **For this Report, the averaged IAS4cc signal using the new gauge factors will be considered the best guess for the current reaching the Outdoor Mode converter. We also assume that the individual monitor calibrations are switched from that derived on Shot 10634.**

IAS1. The four IAS1 monitors record total (anode) current at a location near the High-Bay side of the test cell. In the Outdoor Mode, they are some 11 meters away from the converter, which is located near the roll-up door. In the Shot Header, the four monitors making up the IAS1 location are listed as follows: IAS1000, IAS1090, IAS1180, and IAS1270. The gauge factors listed are the same for all four monitors: 2.75e4 (units). The four IAS1cc waveforms as retrieved from the H3_10433cc.HDF file for Shot 10433 are plotted in Figure 5. Note that a) the waveforms drop below ZERO late in time, the symptom of the 'droop', and b) 3 of the 4 signals group very close together, whereas the 4th one, IAS1090 (RED), is clearly bigger than the other three. The difference in the peak is about 9% in the case of IAS1090. Prior to this Report, a previous study of HERMES full-power shots conducted since starting at Shot 9654, and ending with this shot, concluded two points about the IAS1 signal: 1) the peak in IAS1 has been rising slowly but steadily over ~780 shots; and 2) starting at around Shot 10000, IAS1090 separated from the other 3 IAS1 monitors, and the gap has remained at ~ 9% for a considerable period of time. [Recent Shots (~ 10,500), however, do not exhibit an oversize IAS1090.] The first point will be discussed further in the section below on the MK7 waveforms. The second leads to **Conclusion #1**: **for the purposes of calculating the average IAS1 current (IAS1_AVE), for this Report, IAS1090 will be excluded.** (If the 090 signal is comparable to the other signals, this rule is suspended.) Since the other 3 monitors track each other very closely, when IAS1090 is so excluded, the average is observed to drop by 2-3%. The average is then dedrooped at 275 ns, a number discussed further below in connection with the short-circuit calibration shots. The resultant

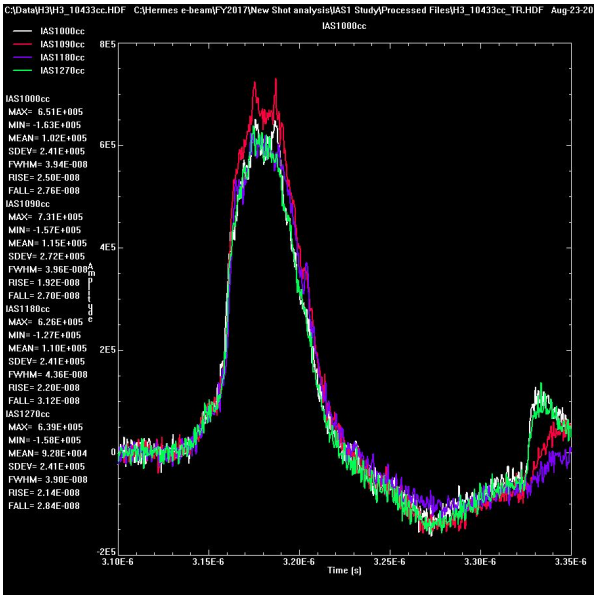

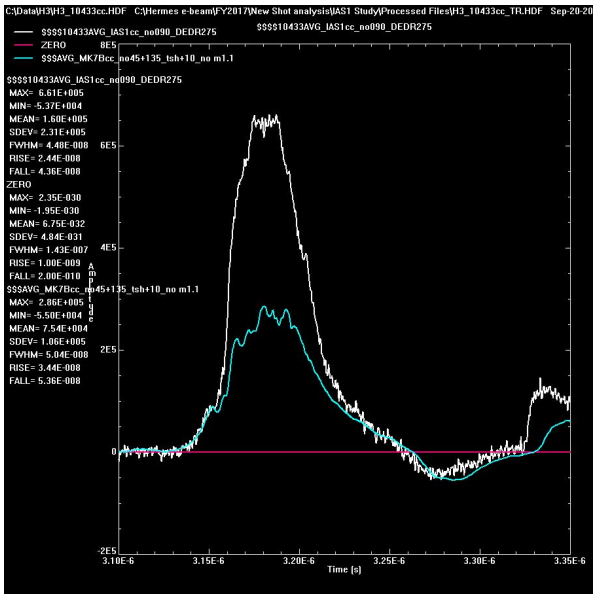

Figure 5: IAS1 individual currents, Shot 10433 **Figure 6: IAS1_AVE and MK7_AVE**

IAS1cc_AVE is depicted on Figure 6 as the WHITE curve. Its peak value (averaged through spikes) is ~ 650 kA. It must be mentioned that with monitor IAS1090 excluded, IAS1cc_AVE peaks at a value often below that of IAS3cc_AVE. Perhaps coincidentally or not, when IAS1090 is included in IAS1cc_AVE, the peak more closely matches that of IAS3cc_AVE. However, when IAS1090 is excluded, IAS1cc_AVE peak

more closely resembles that of IAS2cc_AVE. Hence the conclusion here is that IAS3cc_AVE tends to run slightly high with the current gauge factors in place.

MK7. These are four Bdot monitors (no de-droop needed) located within 10 cm of IAS1 on the inner (cathode) MITL, and so measure the bound current at that location. The FINAL FORM of the MK7cc_AVE processed signal is shown as the light BLUE curve in Figure 6. The peak value of MK7cc_AVE is 286 kA in the plot. Note that 1) the tails of the total and bound currents (e.g. after peak current) track each other quite well, indicating that 275 ns is a good estimate of the de-drooping factor, and 2) the ratio of the bound to the total current is more-or-less constant through the pulse. This reflects the possibility that the diode is running at self-limited impedance. With such a large A-K gap, there is no 'gap closure', and hence the feed impedance should be constant. As will be seen below, the feed impedance is indeed a constant through most of the power pulse.

The form of MK7cc_AVE shown in Figure 6 is the result of a number of Data Interpretation decisions. To illustrate this, we discuss now the result of signal processing after a calibration short-circuit shot taken at half-power, **Shot 10402**, taken in March 2017. Plots of the individual monitor signals are shown in Figs. 7-11 below for the following current monitors (respectively): IAS1, IAS2, IAS3, MK7, and MK6. As stated above, IAS1 monitors are located 2 meters upstream of the Standard Mode converter location. Monitors IAS2 and IAS3 are located very close to the converter location. The MK6 monitors are a set of Bdots located upstream of the MK7 monitors. They are included here for comparison with the MK7 monitors, and are not used for shot analysis. More will be said about the MK6 signals later. The IAS1-3 waveforms have been cable-compensated, but not de-drooped.

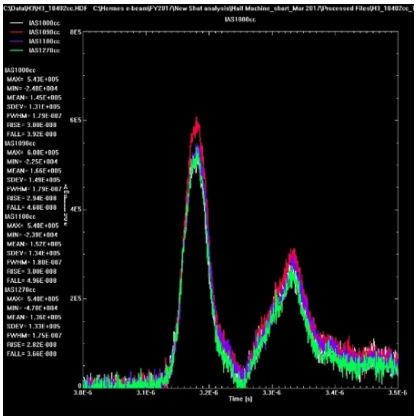

Figure 7: IAS1, Shot 10402

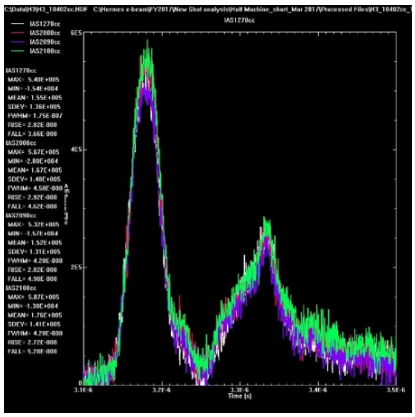

Figure 8: IAS2

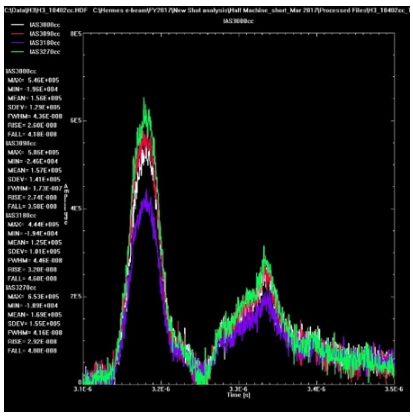

Figure 9: IAS3

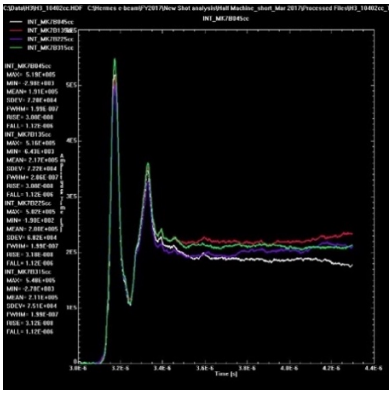

Figure 10: MK7

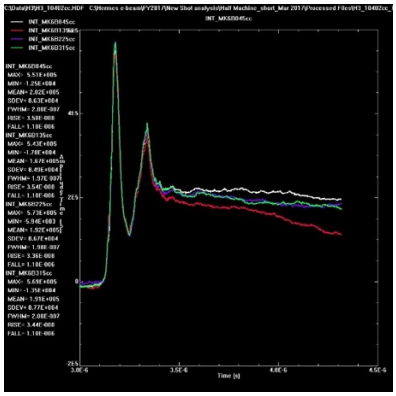

Figure 11: MK6

Here are some qualitative observations about the waveforms in Figures 7 - 11:

Figure 7 (IAS1cc): Here the IAS1090 waveform (RED) is observed to be significantly larger in magnitude than the others (608 kA peak compared to ~ 545 kA for the others, a 11-12% increase). This supports the decision to exclude it from the average.
Figure 8 (IAS2cc): Here the peaks are spread out from a low of 532 kA peak to 587 kA.
Figure 9 (IAS3cc): The variation in peak magnitude is even larger here, from 444 kA to 653 kA. As with IAS2cc, there is no obvious way to exclude any waveform, so all are included in the average.
Figure 10 (MK7Bcc): the 4 waveforms here are very similar in peak magnitude.
Figure 11 (MK6cc): very similar behavior to the MK7 monitors. Note that in both the MK6 and MK7 cases, the 'tails' of the waveforms remain fairly constant in magnitude for the entire duration of the record length. This appears to be a very odd feature of the bound currents.

Note that the **IAS4** and **IAS5** monitor signals are not included in this discussion, because Shot 10402 was taken using the Standard Mode hardware, which does not include those monitors. The IAS4/5 monitors will be discussed separately later in this Report.

The premise of a short-circuit shot is that both the total and bound waveforms should match each other in peak value and in waveform shape. The total and bound current shapes above clearly do not meet that criterion, and either the total currents must be increased in magnitude late in time, or the bound current tails must be decreased. Within XDAMP, there is no obvious way to achieve the latter, but the former can be accomplished by the use of the 'dedroop' command. This is illustrated in the Figures below.

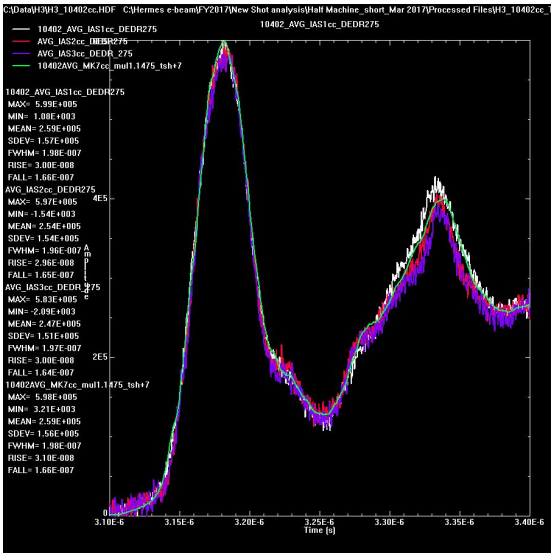

Figure 12: IAS1-3 + MK7

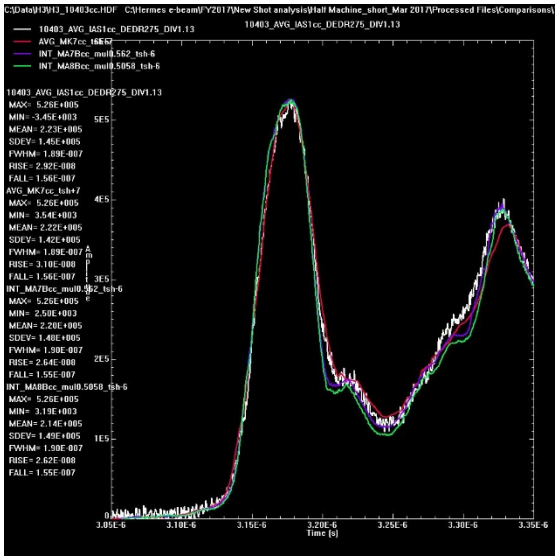

Figure 13

There are four waveforms plotted in Figure 12 above: IAS1cc_AVE, IAS2cc_AVE, IAS3cc_AVE, and MK7cc_AVE. They have been adjusted as follows: IAS1-3 have been 'dedrooped' using time constant = 275 ns; and MK7_AVE have been multiplied by 1.1475 (e.g. about a 15% boost), and time-shifted by +7ns. Using these adjustments, the peak values of the 4 respective waveforms are: 599, 597, 583, and 598 kA. There are several conclusions here: a) despite the variation amongst the four each IAS2cc and IAS3cc

waveforms, when averaged together, IAS2cc_AVE is almost identical to IAS1cc_AVE in peak value and waveform shape, with IAS3cc_AVE lower in peak value from IAS1cc_AVE by less than 3%; and with the ~15% boost in value and the time shift, MK7cc_AVE is almost identical in peak value and waveform shape to the total currents. This is accomplished in the case of the total currents by adding the 275 ns 'de-droop'.

There are also four waveforms plotted in Figure 13 above: IAS1cc_AVE, MK7cc_AVE, and the total currents MA7Bcc and MA8Bcc (see locations in Figure 15 below). The latter are Bdots and are NOT dedrooped. For this plot, MK7cc_AVE is time-shifted but NOT boosted, and IAS1cc_AVE is REDUCED by 13%. The MAxcc currents are time-shifted by -6ns, and multiplied by(respectively) 0.562 for MA7Bcc and 0.5058 for MA8Bcc.With these adjustments, the four waveforms are observed to be almost identical in both peak value and waveform shape. Thus, the same 275 ns dedroop factor results in waveform shape matching for both the bound currents and the non-dedrooped total currents (MA7 and MA8). This is a *mathematical* statement, e.g. the reason for the hang-up in the monitor signals late in time is not addressed. Clearly the argument can be made that these signals imply charge conservation violation at some point. As indicated in Figure 15 below, the MA7 and MA8 monitors are physically located close to the IAS2 and IAS3 monitors, respectively. While the MA7-8 signals can be made to fit IAS1 and MK7 by the mathematical scaling indicated above, the scalings work only for the short-circuit shot, and are not valid for a full-power bremsstrahlung shot. Accordingly, the MA7-8 monitors will not be discussed further.

As will be discussed further below, in order to make use of Eq. 1 to calculate voltages using the total and bound currents at any point in the MITL, the two waveforms, when over-plotted, must match each other in shape early in time (implying lack of MITL turn-on), then separate during the power pulse, then come back together after the power pulse, implying voltage returning to zero. Since the dedroop process for the IAS1-3cc waveforms accomplishes this, at the 275 ns value indicated above, this leads to **Conclusion #2**: **the IAS1-3cc current waveforms will be de-drooped at a value of time constant 275 ns.**

In Figures 12 and 13 above, the MK7Bcc_AVE and IAS1cc_AVE have been increased and decreased, respectively, to make a point. If the purpose of short-circuit shots is to make all the waveforms equal in peak magnitude, this can be accomplished by either a) increasing MK7Bcc_AVE by ~ 15%, or b) decreasing IAS1cc_AVE by the same amount. Without compelling physics reasons for either action, there is distinct ambiguity about which of these actions, or combination of actions, to take.

This Report makes the following conclusion based upon the structure of Eq. 1: the effort on the voltage calculation uncertainty is minimized by changing the size of MK7 instead of IAS1. There are several mathematical reasons for this: a) the first term, at the voltages typical of HERMES shots, dwarfs the second term, the latter term being about 5% of the former, and b) the dominant first term consists of the difference of *squares*. For a typical HERMES shot, the total current is about 3 times the size of the bound current (~600 kA compared to ~200 kA). Thus, the square of the total current is about 9 times the size of the bound current squared. Therefore, decreasing the total current by ~15% leads to a significantly bigger effect on the calculated voltage in the Mendel equation (Eq. 1) than raising the bound current by ~ 15%.

There is also another compelling reason to leave the calibration factors for current IAS1-3 unchanged. In the 2011 timeframe, the author and Bruce Weber of the Naval Research Laboratory conducted an in-situ pulser calibration of what were then called the 'IC' current monitors. These were a set of 6 Bdots arranged in 3 pairs (A, B, and C), with an 'N' and a 'P' leg of opposite polarity. The setup is depicted schematically below in Figure 14. The IAS1 and M8 monitors were also subject to calibration, but their response was judged to be dominated by noise pickup. Since the IC monitors performed adequately in the in-situ calibration process, it was decided to use the IC monitors to calibrate the rest of the current monitors during a half-machine short-circuit shot (Shot 9244). The monitors so calibrated are listed as follows: IAS1, IAS2, IAS3, MK6, MA6B, MA7B, MA6DIF, and MA8B. A new header was devised for shots subsequent to Shot 9244 that incorporates the new gauge factors. For example, the gauge factor for the IAS1 monitors was

reduced from 3.2e4 to 2.75e4, and for IAS2-3 the gauge factor was reduced from 4.18e4 to 3.75e4. These values remain in the current header, and have been in place since 2011.

Setup for calibrating Hermes-III current probes using external pulser (10/10 and 10/11, 2011)

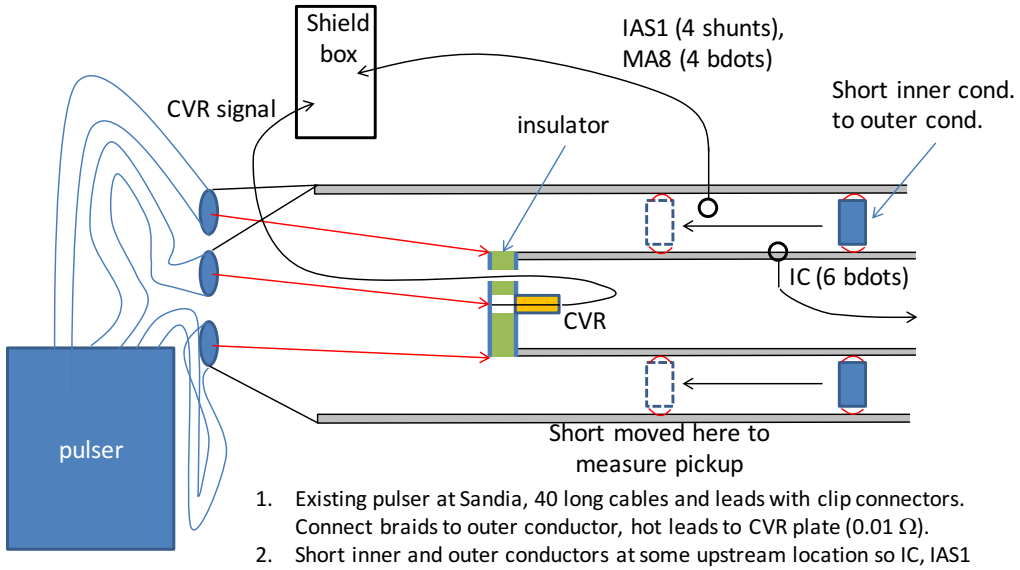

1. Existing pulser at Sandia, 40 long cables and leads with clip connectors. Connect braids to outer conductor, hot leads to CVR plate (0.01 Ω).
2. Short inner and outer conductors at some upstream location so IC, IAS1 and MA8 monitors can be calibrated.
3. Use CVR signal as calibration standard.
4. Adjust other current monitor cals to re-calibrated monitors on short circuit shot with H-III (shots 9244 and 9245).

Figure 14

Full Machine, 67 cm AK gap

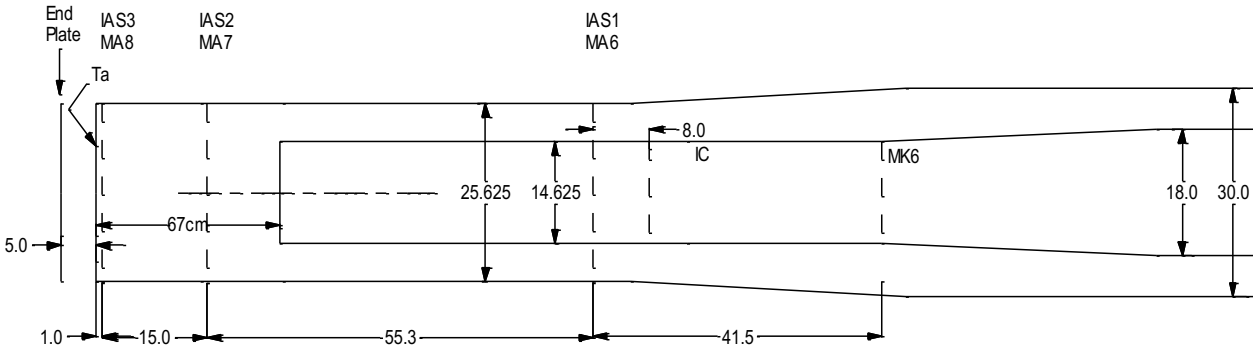

Figure 15. Layout of anode and cathode monitors in the load region (2011 drawing)

The location of the monitors listed above are shown in the schematic drawing of the HERMES load region (Standard Mode) in Figure 15, made at the time of the in-situ IC calibrations done in 2011. Of the monitors listed, IAS1 can be considered the most important total current monitor, and thus is considered as Primary for this Report. The MA monitors are not referred to further for this Report, as they have fallen out of

calibration since 2011. This leads us to **Conclusion #3**: **The IAS1-3 monitor calibrations in place since 2011 will be retained.** In short, the gauge factors for IAS1-3 have *already been reduced*, in 2011, and in the case of IAS1, the reduction was almost 15%.

The discussion now switches to the history of the development of the MK7 bound current monitors. These monitors were mentioned as the bound current monitors closest to the IAS1 total current monitors, and are therefore used to estimate the voltage at the IAS1 position. The MK7 monitors were mentioned in connection with recent short-circuit data, and the question of whether the IAS1 signals should be decreased in size, or the MK7s should be increased. That question was partially resolved in the previous paragraph, e.g. leave the current IAS1-3 gauge factors in place. But that discussion involved a previous adjustment to the IAS1-3 gauge factors that used the IC monitors (bound current) as a reference. The next question then must be asked: what is the relation between the IC and MK7 monitors? This, as it turns out, is a complicated question.

In the time period shortly after the short-circuit Shot 9244 mentioned above, the 'IC' monitors were replaced with the 'MK7'-designated signals. The last HERMES shot with IC signals listed in the Header was 9654, and the first shot with MK7 in the Header was 9680. The 9654 Header lists the following 6 signals with IC labels and their V/DIV value: ICBN – 7.54e11, ICCP – 7.4e11, ICAP – 7.75e11, ICAN – 7.92e11, ICBP – 7.25e11, and ICCN – 7.14e11. The listed V/DIV values reflect the revised calibration values for the N and P sides of the 3 A, B, and C monitors from the pulser exercise discussed above. In the Header for 9680, the first two signal names still appear – but they have been 'commented-out' of the Header. The last 4 IC names have been replaced by, respectively, MK7B045, MK7B315, MK7B225, and MK7B135. The same two commented-out signals names and 4 MK7 names appear in Headers up to the present time. The naming convention for MK7 implies that there are 4 monitors equally spaced in azimuth at the MK7 location. But the calibration factors, while taken from the IC monitor signals, use only 4 out of the 6 original IC names, and only one of the original pairs (A). A cursory examination of the values for the IC-to-MK7 signals indicates a > 20% increase in peak magnitude on Shot 9680 compared to 9654. After that, there is a trend line downward over the next 1-20 shots, suggesting some on-the-fly changes to the MK7 monitor setup. Thus, although the MK7 monitors appear to have replaced the IC monitors (as the author was informed at the time), the mapping from 6 to 4 monitors is not clear. There is even some sentiment for the idea that the MK7 monitors are unrelated to the IC monitors (Ken Mikkelson, private conversation). There is no known documentation for the transition in setup from the IC to the MK7 monitors, so we are left with making some kind of *ad hoc* determination.

One approach is simply to make use of the result of the half-machine short-circuit Shot 10402, whose waveforms were discussed in Figures 4-10. That is, if the IAS1-3 calibration factors are to be left alone, then the option exists to simply raise the MK7 calibration values by 10%. This subject will be more extensively visited further below, in the discussion of how to extend the voltage contours derived from the Mendel Equation (Eq. 1) visible in Figure 1 to 19 MV. For right now, we state the conclusion as another **Conclusion #4**: for this Report, **The MK7 monitor calibrations in place since Shot 9680 will remain unchanged.** In the ensuing discussion, it will be shown that whether a 10% increase in MK7 calibrations is executed or not, the effect on the resultant voltage determination is slight.

If the ambiguity in the origin of the MK7 signals were not enough of a concern, the behavior of these monitors during full-power HERMES is also problematic. The processed bound current for one of these shots (10433) is shown (light blue) in Figure 6. The individual four MK7 waveforms for this shot are shown below in Figure 16. As can be seen, their peak magnitudes vary widely. The MK7B135cc signal (RED), for example, exceeds 500 kA. The author has studied the behavior of the individual MK7 (and MK6) monitors using a sampling of shots from 9800 to the present. During this time, the MK7B135cc signal has varied from ~ zero to over 800 kA. The MK7B045cc signal has been observed as high as 500 kA, and often

exceeds the peaks seen on the MK7B225cc and MK7B315cc monitors. Over the span of shots that are the subject of this Report – 10268 to 10313, the latter two monitors (225 and 315) have behaved the most consistently. This has occurred even as the total current monitors, IAS1 to 3 – have shown good reproducibility over each set of 4 monitors, except for the variations already noted. It is clear, then that in

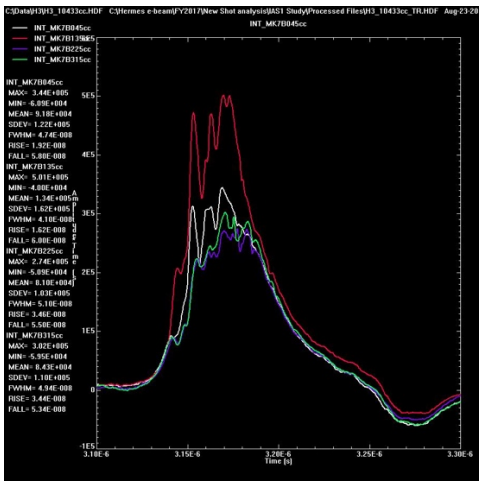

Figure 16: MK7, Shot 10433

many if not most shot cases, some number of the MK7 individual signals must be left out of the average. Which ones should be deleted amounts to a judgement call, although one that can take into consideration the previous history of what the bound current 'should be' on a HERMES shot. For example, there is accumulated evidence from historical HERMES shots (Ken Mikkelson, private conversation) that out of a *total* current of ~ 600 kA, ~ 400 kA is *flow*, and ~ 200 kA is *bound* current. As will be discussed later in this Report, a level of ~200 – 300 kA for bound current is consistent with expected voltage, and expected positioning of HERMES shots in the extended $Z_oI_c - Z_oI_a$ plot that will be derived below. This leads us to another **Conclusion #5**: **for this Report, The MK7 average peak value will be assumed to be in the 200-300 kA range.** This conclusion guides the decision on which MK7 individual signals to keep, and which to delete from MK7Bcc_AVE. Note that this does NOT mean that MK7Bcc_AVE can never exceed 300 kA. There is some anecdotal evidence, for example, that in the time between Shots 9800 and present shots, the level of peak bound current has been slowly dropping with time. Earlier shots in this period, even with MK7B045 and MKB135 removed from the average, tend to peak in the 280-290 kA range, whereas more recent shots have peaks more in the 220 kA range. In the Outdoor shot series discussed in this Report, a majority of shots have the 045 and 135 waveforms removed from their MK7Bcc_AVE signals. In a few cases (ex. 10275), only the 315 waveform has been retained. This decision is connected to **Conclusion #4.** Adding in a 10% to the MK7 signals has tended to increase their average peak value to > 300 kA, and so this suggested augmentation based upon Shot 10402 (short-circuit) has been dropped.

The MK6 bound current monitors were also featured above, in Figure 11. These monitors (see Figure 15) are located upstream of the Mk7 and IAS1 monitors. While their response in the short-circuit shot compares favorably with the MK7 monitors, on a full-power HERMES shot, their behavior is significantly less consistent. In the earlier shots closer to 9800, their peak magnitudes are comparable to the MK7 monitors, their wave-*shape* is radically different. Attempts to use the MK6 waveshape for the bound current on a particular shot do not yield consistent results. (See the discussion on comparisons with dose-rate monitors below.) Furthermore, on more recent shots, the individual MK6 signals, while displaying more consistency than the MK7 ones, peak at a considerably lower level than the MK7s, typically ~ 150 kA. The shapes of the signals also display a flat-top profile, rather than the more rounded maxima of the MK7 signals, possibly an indication of some kind of signal interruption like a short. A peak bound current value of 150

kA is considerably below what can reasonably be expected of the HERMES bound current, as will be more completely explained below. For this reason, the MK6 signals are not used to calculate the shot voltage using Eq. 1.

IAS4 and IAS5. The last current signals to be addressed here are the monitors closest to the converter in the Outdoor mode that is the subject of this Report. These are IAS4 and IAS5 monitors. They are positioned (two monitors at each location) on a large flange mounted on the end of the Outdoor Mode hardware, within a few cm of each other, and within a few cm of the converter. The flange is the leftmost piece of hardware visible in the panoramic photograph of the Outdoor hardware. They have functioned as the best estimator of the current reaching the converter since the Mode itself was devised. On a typical HERMES Outdoor Mode shot, out of the ~ 600 – 650 kA measured at IAS1, the IAS4 monitors using the present gauge factors record ~ 350 kA, and the IAS5 monitors ~ 325 kA, i.e. slightly less than at IAS4. Given the proximity of the IAS4 and IAS5 monitors, this difference is likely due to difference in monitor calibration. The ~ 300-350 kA difference represents current that is shed along the entirety of the Outdoor Mode hardware. Besides the IAS4-5 monitors, there is a set of individual monitors known as 'XMB'. They are periodically spaced monitors located on the west side of the outer MITL in the section to the right of the converter. In the panoramic photograph, the largest-diameter outer MITL section is visible in roughly the center of the photograph. To its left is a smaller-diameter section with the periodically spaced XMBs. In the photograph, their location is visible as a series of slightly darker small circular features in this smaller-diameter section. On a typical HERMES outdoor shot, these monitors register a value higher than the IAS4-5 monitors, and below the IAS1 current, typically in the 450-500 kA range. Comparison of the XMB peak values observed in sequence from right to left shows a decline as the converter is approached. All these readings are consistent with a continuous current loss as the current proceeds down the MITL, from far right in the photograph to the far left. TLD readings also indicate a preferentially higher current loss to the top side of the MITL, compared to the bottom. This is presumably caused by the droop in both inner and outer MITLs.

These observations are qualitatively consistent with a considerable current loss associated with the present Outdoor Mode hardware. Unfortunately, these are not quantitative conclusions. That is because ***neither the XMB nor the IAS4-5 monitors had ever been calibrated***, at least prior to Shot 10458 (see below). In the case of the IAS4-5 monitors, the Header records their gauge factor as 3.75e4, the same as the IAS2-3 monitors. But these gauges are notional only, and were devised because the IAS4-5 monitors are observed to be of the same design and construction as the IAS2-3 monitors. (As a corollary, if the IAS2-3 monitors are judged to need de-drooping, then so do the IAS4-5 monitors.) Calibration shots (short-circuit) on HERMES have only been taken with the Standard Mode hardware. Then prior to Shot 10458, the amount of current reaching the converter, and therefore the amount of dose to be expected, has been unknown.

The IAS4-IAS5 monitors were calibrated on a short-circuit shot (10458 – July 2017) taken as part of the Ion Diode Test Series associated with the Neutron Generation LDRD Project. The reason is that the large flange containing the IAS4-5 monitors was assembled into the ion diode load region (for fit convenience). The load hardware was re-arranged slightly in order to execute the short-circuit shot, since the IAS4-5 monitors are not used for Ion Diode load shots. A second short-circuit shot (10634) was taken using the same hardware, as part of the April 2018 Ion Diode shots series. This second shot yielded more consistent data, and thus will be the focus of the discussion below.

One slight caveat is that the peak current(s) on both shots (10458 and 10634), at 470 kA, were reduced compared to the previous short-circuit shot discussed above (10402). The reason for this is not known at present, although it is pointed out that Shot 10402 had a different set of load hardware from the Ion Diode short-circuit shots. The lower indicated peak current might suggest that Shots 10458 and 10634 did not behave as fully short-circuit shots. However, in both Shots 10458 and 10634, and as had occurred previously with Shot 10402, the MK7Bcc_AVE waveshape matched that of IAS1cc_AVE, and the peak

value of MK7Bcc_AVE was ~10% below that of IAS1cc_AVE. Therefore, the shot is assumed to function as a standard short-circuit shot. So that the 4 IAS4/5 monitors signals would be included in the standard H3xxxxcc.HDF file, the cables attached to these monitors were installed in place of the IAS2-3 cables.

We first plot the (2) individual waveforms making up averages for both the IAS4 and IAS5 monitors. These are displayed in Figures 17 and 18 below. All waveforms are de-drooped at 275 ns. As can be seen, the two signals (060 and 240) for each monitor set are very similar in size to each other. Each set of waveforms is then averaged to form IAS4cc_DEDR275 and IAS5cc_DEDR275, respectively. These are then plotted compared to IAS1cc_AVE (WHITE) in Figure 19 below. Here, IAS4cc_AVE is plotted in RED, and IAS5cc_AVE in lt BLUE. It is immediately obvious that a) both IAS4 and IAS5 are too large compared

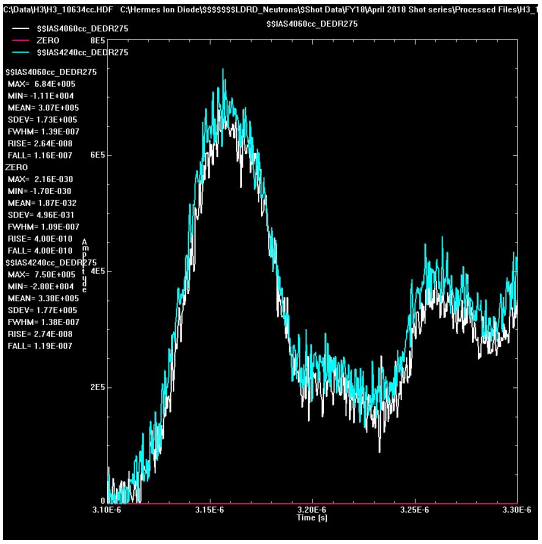

Figure 17: 10634 IAS4

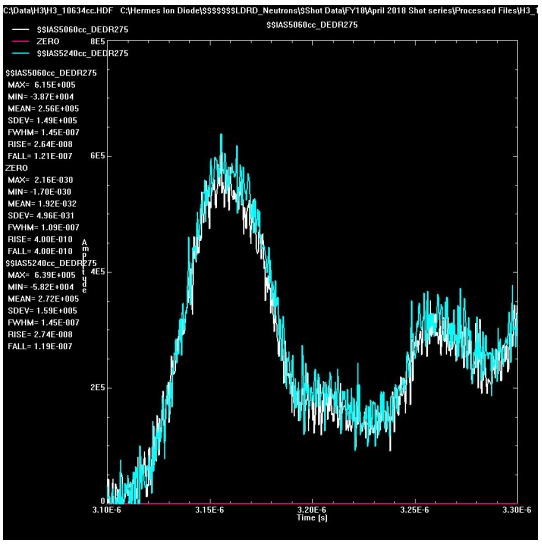

Figure 18: 10634 IAS5

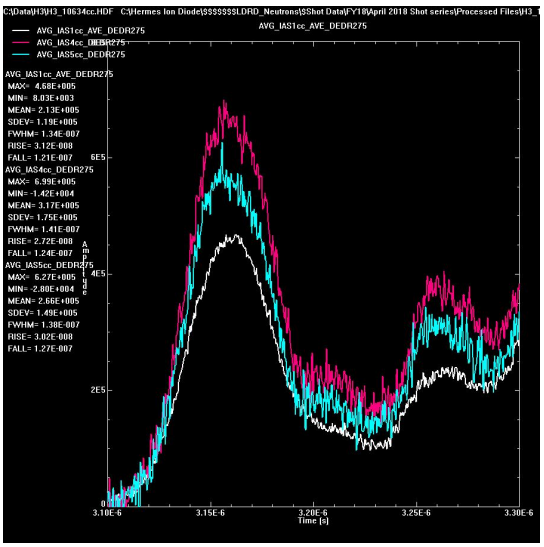

Figure 19: 10634 IAS 4-5 and IAS1

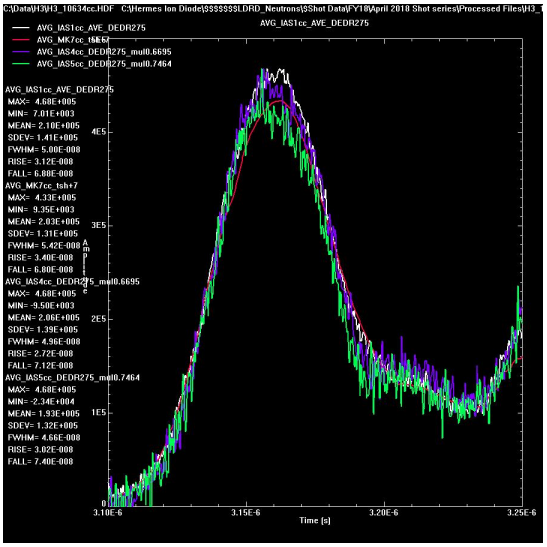

Figure 20: 10634 IAS 4-5, IAS1, MK7

to IAS1cc_AVE, and thus each monitor set must have its calibration factors lowered. And since IAS4cc_AVE peaks higher than IAS5cc_AVE, its calibration factor must be lowered more than IAS5cc_AVE. If now IAS4cc_AVE is multiplied by **0.6695**, and IAS5cc_AVE by **0.7464**, the resulting

modified waveforms are plotted together with IAS1cc_AVE and MK7Bcc_AVE in Figure 20. Use of the two respective scale factors results in a reconciliation of the IAS4 and 5 current waveshapes with the IAS1cc_AVE signal. For comparing converter current with IAS1cc_AVE, either one of IAS4 or IAS5 waveforms can be used. For this Report (and subsequent Summary of a later Outdoor Shot Series, 10649 – 10711), the IAS4cc_AVE waveform, multiplied by 0.65, is what is used to estimate the converter current.

An earlier analysis was done for the short-circuit shot taken prior to Shot 10634, taken during the July 2017 Ion Diode test series. That was Shot 10458. While several puzzling aspects of that shot were identified, the net result of analyzing the IAS4 waveforms is that the same conclusion is reached, namely that the two different IAS4 waveforms are averaged, then multiplied by 0.65. This is then the value that is noted for the outdoor shots in this Report, and for the subsequent series (10649-10711) as well. As will be noted later in this Report, when considering IV^x scaling of the indicated voltage and current at the IAS4 location, this yields a relatively good outcome. That is, when $IV^{1.1}$ is calculated for the present shots using the new IAS4_AVE waveform and time-shifted voltage at IAS1, the scaled waveshape follows the shape of SCD very closely. This then leads us to **Conclusion #6**: **for this Report, the averaged IAS4cc signal using the new gauge factor (0.65) will be considered the best guess for the current reaching the Outdoor Mode converter.**

There is a final detail to be discussed before making use of the IAS4 current monitors. These signals are listed in the Shot Header, but not in the H3_xxxxxcc.HDF XDAMP file. They ARE listed in the non-cable compensated XDAMP file H3_xxxxx.HDF. To derive the cable-compensated signals requires a separate procedure. This is true of any non-cable compensated signals, not just the IAS4s. The procedure is listed in Appendix 2, and was derived by Victor Harper-Slaboszewicz. It is hoped that one day, this *ad hoc* procedure can be incorporated into the H3_xxxxxcc.HDF file itself. The example used in the Appendix text is the signal for one of the XMB current monitors. These monitors are uncalibrated at present, and so are not addressed in this Report.

Dose-rate X-ray monitors. There are three x-ray monitors routinely fielded on HERMES shots. They provide dose-rate data to supplement the time-integrated TLD monitors. At present, these monitors are not absolutely calibrated, and so provide qualitative waveshape data. If TLDs were fielded next to the monitors themselves, the dose-rate could be absolutely calibrated.

The first monitor is PIN (or PINB). This is a P-I-N diode located on the Test Cell back wall on the north side of the roll-up door, ~ 10 degrees off the MITL main axis. For full-power Standard Mode shots, PINB is in the near-axis radiation field, and dose-rate tends to scale with $IV^{2.2}$. But for the Outdoor configuration, the PIN location lies at near-90 degrees. Extrapolating from RITS-SMP experiments, at this angle the scaling would be expected to be with lower power than $IV^{2.2}$, more like $IV^{1.1 - 1.5}$.

The second monitor is the SCD (Spherical Compton Diode), which is fielded on a movable support that is typically placed at ~ 45 degree angle to the converter, and approximately 30-40 cm away. With this placement, the IV^x scaling should be similar to that for PINB. As will be shown later, with x set to 1.1, the scaled SCD waveform for most of the shots in this Report fits IV^x scaling very well. While this is a relative measurement due to the scaling, if TLDs were routinely fielded on the front of the monitor, this could become an absolute dose-rate monitor. The PINB signal scales with a few of the shots, with x set to 1.8. But it is clear from PINB-SCD waveshape comparisons that PINB detects some MITL losses that are not seen by SCD. It may be that the positioning of SCD, in front of the converter, makes it insensitive to losses in the MITL section in front of the converter, which can be readily detected by PINB. It should be

also noted that while the PINB monitor has been in place for many years, the SCD has not always been the *same* SCD, due to unit breakage. Again, with an accompanying TLD with every shot, dose-rate can be calculated absolutely, independent of the particular SCD unit being used.

The third monitor, SCDREFcc, is less relevant for the Outdoor shots. This is a Spherical Compton Diode that is suspended on a boom located above and forward of the converter at the Standard Mode location. This positions it at an approximate 45 degree angle for Standard Mode shots. For Outdoor shots, however, the monitor is quite far from the converter position, so its performance is not consistent in the shots detailed in this Report.

Of the three dose-rate monitors, since the SCD monitor is movable, and always placed in the same orientation with respect to the converter, its signal can be compared between shots in all three HERMES mode shots, Standard, Extended, and Outdoor. It will be the subject of detailed comparison with the converter current and faceplate TLDs, in the discussion below.

4. CHARACTERIZATION OF TOTAL CURRENT, VOLTAGE, AND FACEPLATE TLD DATA, SHOTS 10268 – 10313.

Data from this Outdoor series will be presented in the following sections:

1) **General description of parameters in the 45 shots**. The format will be x-y plot form, with the x-axis indicating the number of shots (45), and the y-axis the particular parameter that is the subject of the plot. These plots are general characterizations that give graphic depictions of reproducibility, for instance. In the case of reproducibility, the exact calibration accuracy of the data is secondary, as the same analysis protocol was used for each shot. The x-axis is simply labeled by the number of shots, not the shot numbers themselves, in the interest of saving space. Shot number 1 is then Shot 10268, and proceed in sequence till number 45 (Shot 10313). The lone Shot not included is 10283, for which no H3_xxxx.HDF file is posted to STL.

2) **The total and bound currents, plus the resulting voltage at IAS1 calculated from them, is characterized by plotting on an extended version of Figure 1 (Ottinger 2006).** Recall that Figure 1 plots the set of solutions to Eq. 1 which, when plotted in Z_0I_c-Z_0I_a space, yield a set of hyperbola-like curves. Since the earlier work is limited to voltages below 10 MV, a prescription is presented in which the hyperbola curves are extended to the 19 MV level. Then shot data (peak values of total (IAS1cc_AVE), bound (MK7Bcc_AVE)) are plotted on the voltage contours. As will be seen, this exercise gives a connection of the HERMES data to MITL theory, and helps provide heuristic insight into the likely validity of the V-I data.

3) **Scaling of the 45-shot TLD data, taking both voltage and current into account.** The approach here is to assume the validity of Radiographer's Equation inversion, which connects dose-rate of photon radiation to IV^x scaling, where V is the voltage at the converter in MV, and I is the converter current in Amperes. This inversion implies that the 'x' in the formula is a constant, which in turn implies that the electron angle(s) on the converter, whatever they may be, remain fixed for the duration of the power pulse. It will be shown that

    a. taking both voltage and current on a given shot reduces the data scatter significantly. This means that the variation in say the faceplate TLD data can largely be accounted for by considering the variation in the HERMES power coming forward on a given shot.
    b. While the calibration of the dose-rate monitors (PINB and SCD) have not been characterized, the relative size of, in particular, the SCD monitor, tracks the photon dose of the shots relatively well. That is, if the SCD waveshape is time-integrated and compared to the summation of the 29 faceplate TLDs, the ratio of the two is roughly constant (more on this point later). In addition, the (scaled) SCD waveshape compares very closely the IV^x waveshape for a given shot, where x = 1.1. And finally, if the IV^x waveshape for a given shot is time-integrated, and divided into the faceplate summation for the same shot, the ratio is relatively constant. And while Standard Mode shots are not the subject of this Report, if the same ratio of faceplate summation and time-integrated IV^x is performed for representative Standard Mode shots, the value of that ratio is roughly equal to that obtained from the Outdoor shots in this Report. This is a very important point. A key assumption of this exercise is that the voltage at IAS1 waveform propagates unchanged, both in peak magnitude and in waveshape. This assumption is validated by the QUICKSILVER simulations of the Outdoor Mode shots.

Therefore, the only variation in IV^x between the Standard and Outdoor Mode shots is the I, e.g. the converter current. This means that the decrease in the overall faceplate TLD magnitudes, compared to the TLD values for shots in the Standard Mode, can be mostly if not entirely accounted for by the indicated loss in current suffered between the IAS1 and IAS4 locations (about 60%). There is a caveat to this statement, however. The 'x' in the above scaling is assumed to be the same for both Standard and Outdoor Mode shots. This is consistent with the electron angle(s) on the converter predicted from QUICKSILVER simulations, but for this Report, this remains an assumption.

4a. General description of parameters in the 45 shots.

We begin by plotting the behavior of the total current IAScc_AVE and voltage at IAS (V at IAS1) for the 45 shots. They are respectively plotted in Figures 21 and 22 below. The peak IAS1 current is seen to be ~ 650 kA, with a ± 4% spread in the majority of the data. Some 6-8 shots (13 – 17% of the total) are outliers, with the lowest peak current at 550 kA (10277). Such outliers are typically ascribed to HERMES pulse power issues (late switches, larger-than-normal switch spreads). In Shot 10277, for example, the TL spread was quite large at 80.5 ns. The voltage at IAS1 (Figure 20) shows a similar spread around the ~ 18.5 MV peak value. Overall, over the 45 shots, there is no indicated systematic trend either upward or downward in the V-I values.

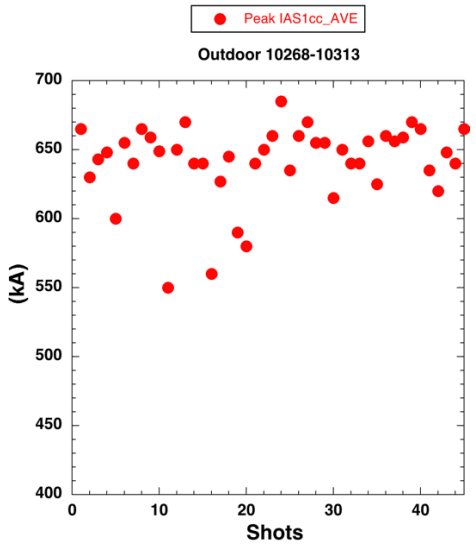

Figure 21. Peak IAS1cc_AVE

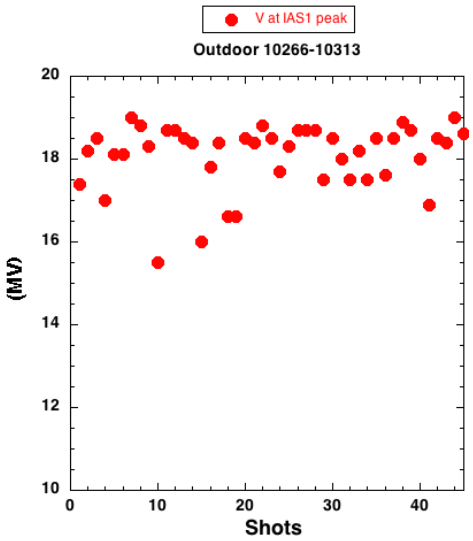

Figure 22. Peak Voltage at IAS1

The overall photon output to the faceplate, as indicated by the 29 faceplate TLDS, will be characterized in two different ways. To illustrate the physical layout of the faceplate TLDs, a typical faceplate readout is shown in Figure 23 for Shot 10256 (not a shot studied here). The faceplate TLDs are arranged in radial positions (7 in all), with equal spacing at each radius, and with the largest-radius position at 24 cm. Such plots have been recorded for every HERMES shot since Shot 9855, and are available on the 1342 Sharepoint site under HERMES_shot_info (BOOM2).

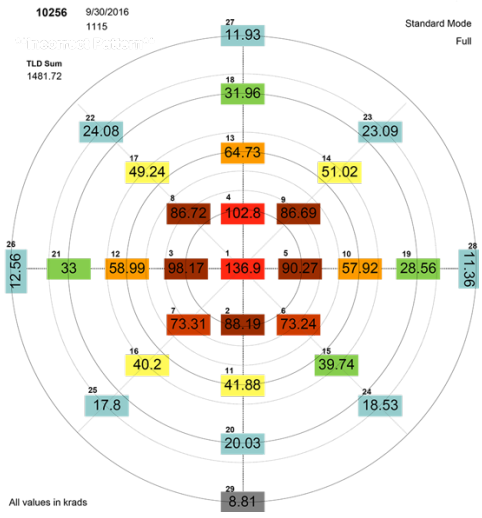

Figure 23. Readout from 29 TLD faceplates TLDs, Shot 10256

The first summation procedure for the 29 TLDs is simply to add up the values of each TLD. This summation is called 'TLD Sum', and is also recorded for every HERMES shot. TLD Sum for Shot 10256 is visible in the upper left of the Figure above (= 1481.72). One observation of this TLD weighting procedure is that it tends to overemphasize the center TLD, labeled at 136.9 krads in the Figure above. For shots such as this one, with dose peaked at the center, the center TLD can contribute as much as 15% to the total TLD Sum.

An alternative method is to 'weight' each radial array by the area of the 'ring' in which that TLD resides. Thus, as the radius of each ring increases, the area increases by the radius r. This approach may be termed the 'dose-area weighted average'. To calculate this weighting for each shot, the Author has adopted the approach of Bruce Weber of NRL (with thanks). One immediate effect of this kind of weighting is that the center TLD, which figures prominently in TLD Sum, is here given NO weight. Mathematically, that is because the center TLD occupies NO area. In order to test the efficacy of this approach, anecdotal calculations were made in which the center TLD was given an effective radius of 1, 2, and 3 cm. Note that a radius of 3 cm is halfway to the first ring of TLDs (radius = 6 cm). It turns out that even with a 3 cm-radius weighting, the center TLD still contributes only about 5% to the total dose-area weight average. Using the Weber protocol, dose-area weighted averages were calculated for all 45 shots, in units of Grays (1 Gray = 0.1 krad). More details about the similarities and differences with TLDSum and dose-area weighting of the Faceplate TLDs is discussed in Appendix 1.

Plots of TLD Sum and Dose-area weighted average are shown in Figures 24 and 25. As can be seen, there is quite a bit of scatter in the data in either plot, with perhaps slightly less spread in the dose-area weighted average data. This scatter is considerable bigger than the variation in the current reaching the Outdoor converter, indicated by IAS4cc_AVE. Plots of the peak value of IAS4cc_AVE, and time-integrated IAS4cc_AVE (delivered charge) are shown respectively in Figures 26 and 27. (Interestingly, while the peak IAS4cc_AVE values do not show any obvious upward or downward trend, the charge delivered to the converter appears to fall slightly with time.)

The reason for the increased variation in dose, compared to delivered current, is simple. Radiation output for bremsstrahlung diodes scales as IV^x, where x is some power between 1 and 2.5. In an IVA, the delivered

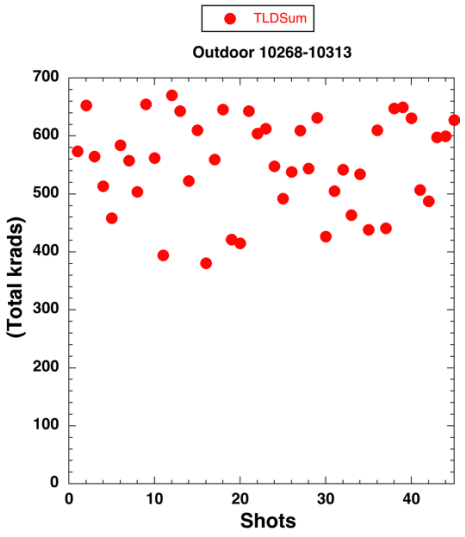

Figure 24. TLDSum

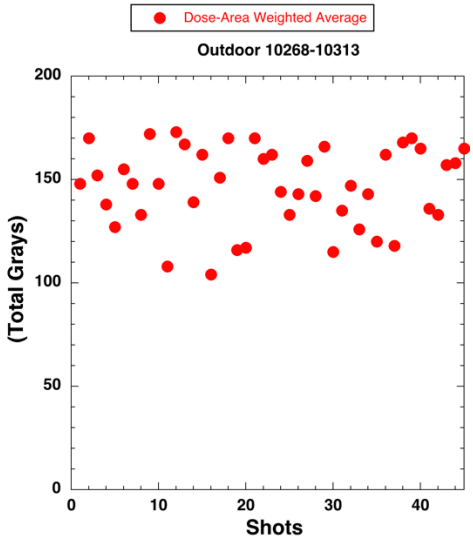

Figure 25. Dose-area weighted average

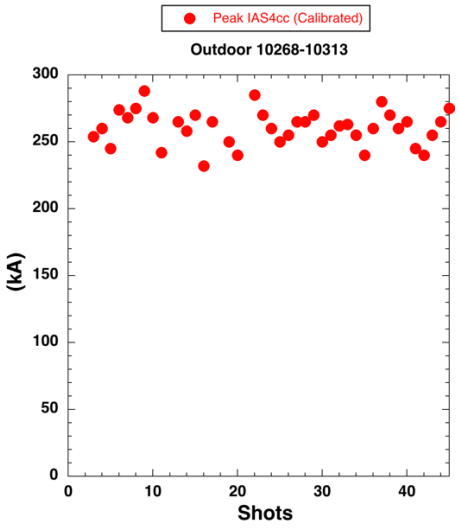

Figure 26. Peak IAS4cc_AVE

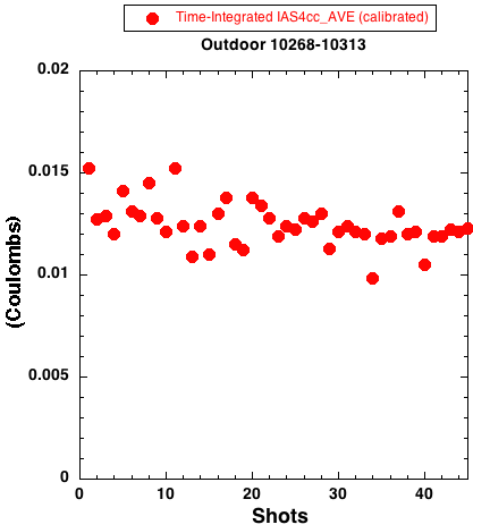

Figure 27. Time-integrated IAS4cc_AVE

voltage scales with delivered current (e.g. V at IAS1 is largely dependent upon IAS1cc_AVE). This means that dose scales at least as I^2, and probably even a higher power. For example, in the afore-mentioned Shot 10277, IAS1cc_AVE peaks at 550 kA, some 15% below the long-term current trend for this series. But in addition, V at IAS1 peaks at only 15.5 MV, an additional 16% below the voltage trend. This leads to the much larger scatter in the dose data seen in Figures 24 and 25.

4b. The total and bound currents, plus the resulting voltage at IAS1 calculated from them, are characterized by plotting on an extended version of Figure 1 (Ottinger 2006).

In this section, we plot the relationship between the total current Ia (IAS1cc_AVE), bound current Ic (MK7Bcc_AVE), and load voltage (Vat IAS1 timeshifted to IAS4 position). The utility of this exercise is two-fold:

1. the HERMES data are tied to a larger picture of MITL operation based upon theory (Mendel plus the Ottinger-Schumer modifications).
2. The placement of peak Ia and Ic values on the voltage contours (extension of Figure 1) yields insight into the relative importance of error in the determination of Ia and Ic.

The importance of the second point goes back to the previously discussed **Conclusion #5**: **for this Report, The MK7 average peak value will be assumed to be in the 200-300 kA range.** The rationale for this conclusion goes back to the results of the short-circuit shots that were the basis of determining gauge factors for the various currents (Shot 10402 and 10458). In both shots, there is a 10% discrepancy between the peak of IAS1cc_AVE and MK7Bcc_AVE. The decision was already made to a) leave the IAS1 gauge factors unchanged (**Conclusion #3**), and b) leave the MK7 gauge factors unchanged (**Conclusion #4**). On the face of it, these two conclusions seem to be contradictory, since it would appear that at least *one* of these gauge sets should change. This exercise presents evidence that the difference between a zero and 10% change to the MK7 gauge factors does not make that much difference to the ultimate voltage determination. This will be detailed below.

In order to extend Figure 1 to the HERMES voltage regime, two features of the plot need to be extrapolated beyond the 10 MV indicated contour in the Figure: 1) the voltage contours, and 2) the 'minimum-current flow' line. The prescriptions for the extrapolating are given in the Ottinger 2006 paper. To determine the voltage contours, Z_oI_a must be related to Z_oI_c for a fixed voltage. This is given in Eq. 20 of the Ottinger paper:

$$Z^2_0I_a^2 = Z^2_0I^2_c + e^2Z^4_oI^4_c/g^2m^2c^4\left(1 - \left[1 - 2gmc^2V/Z^2_0I^2_c\right]^{1/2}\right)^2 \qquad (2)$$

where g is again of order 1. Now in the Ottinger 2006 paper, the value of g as a function of voltage was determined from particle-in-cell (PIC) simulations. For the current discussion, we have to substitute an educated guess as the value of g as the load voltage is pushed to 19 MV. [Later in this Report, results of recent LSP simulations in which g is determined self-consistently will be presented.] It was determined in the 2006 paper that at the 8 MV level, g = 0.8. and this has been the value of g used by the Author to analyze RITS-6 shots at the 8 MV level. As the voltage is raised, g tends to rise slowly. An educated guess as to the value of g at the 16 MV level as been provided by Paul Ottinger (private conversation) at g = 1.2. Then the values of g for voltage intermediate between 8 and 16 MV are set for this Report by interpolation. That is, in Eq. 2 above, the value of g has been set to the following values: for 7-8 MV, g = 0.8, for 9-10 MV, g = 0.9, for 11-12 MV, g = 1.0 (the Mendel default value), for 13-15 MV, g = 1.1, and for 16-18 MV, g = 1.2. This may be considered as somewhat arbitrary, but recall that at HERMES voltage values, the second term of the Mendel equation (Eq. 1) amounts to about 5% of the total voltage, so that these adjustments to g may be considered a second-order effect.

In order to construct the voltage contours, discrete values are chosen for Z_oI_c and solved for Z_oI_a. Enough points are chosen so that the resulting contours (plotted using KaleidaGraph software) appear reasonably smooth. To obtain the values for the minimum current values at the same voltage contours, we use Eq. 23 from Ottinger:

$$I_C^{MC}(V) = \left(gmc^2/4eZ_o\right)\left[-1 + 20eV/gmc^2 + \left(1 + 4eV/gmc^2\right) x \left(1 + 16eV/gmc^2\right)^{1/2}\right]^{1/2} \quad (3)$$

For each voltage contour, the voltage is input into the equation, and then solved for Z_oI_c. The resulting voltage contour set and minimum current line is plotted in ZoIc – ZoIa space in Figure 28 below. This plot should be compared to Figure 4. The data appear plausible and consistent with the data in Figure 4. The lack of smoothness in the voltage contours, and slight jerkiness in the minimum current line are due to the use of discrete plot points, and to the discrete change in g as the voltage is increased. The positions of the curves in Figure 28 can be expected to be refined in future PIC simulations, where in particular the value of g can be determined more accurately.

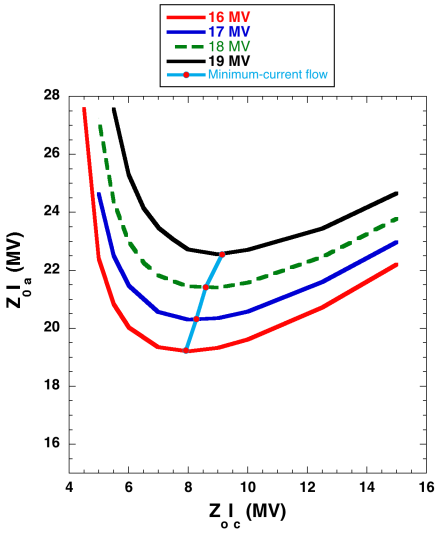

Figure 28

Once the voltage contours and the minimum current line are determined, the values for peak total and bound current on the 45 shots can be added to the plot. This is done in Figures 29 and 30 below.

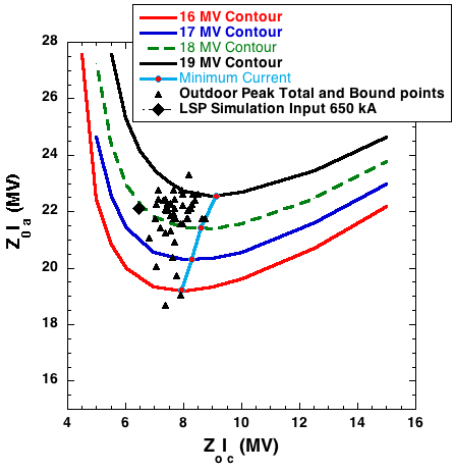

Figure 29

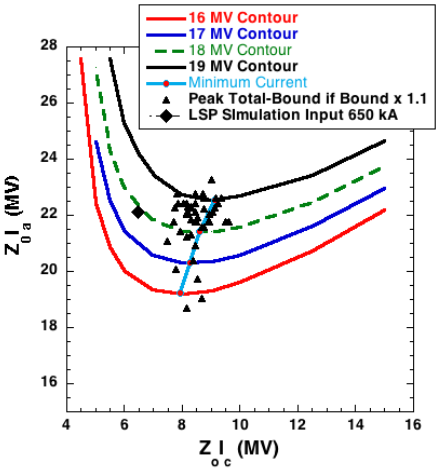

Figure 30

The shot data are plotted two different ways. The first set of points (Figure 29) is derived assuming that the bound current average (MK7Bcc_AVE) is *not* multiplied by 1.1 (e.g. 10% boost), but is used as-is from the cc data file. The second set of points (Figure 30) assumes that MK7Bcc_AVE is boosted by 10%, to be

consistent with the results of the short-circuit shots (10402 and 10458). Without the 10% boost to the bound current, the shot data set are observed to lie to the left of the minimum current line, whereas with the 10% boost, the data fall more squarely in line with the minimum current line. It should be pointed out, however, that the general placement of the shot data from HERMES lies in a vertical orientation, whereas the minimum current line, as in Figure 1, is decidedly tilted. Thus, there does not seem to be an organic connection between the data and the minimum current line.

The placement of the HERMES data can be viewed from a different perspective, as illustrated by Figure 31 below:

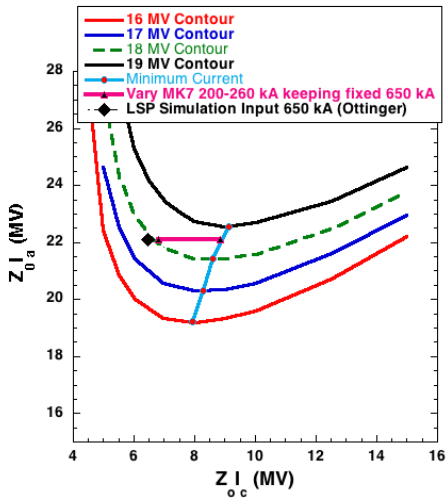

Figure 31

In this plot, the MAGENTA curve is constructed by varying the HERMES bound current (full power) between 200 and 260 kA, while keeping the total current fixed at 650 kA. This range describes the general uncertainty in the bound current MK7Bcc_AVE stemming from the question of the 10% boost. The key observation is this: the data lie in the area around the minimum current line, where the voltage contours are relatively constant in the horizontal direction. So, for instance, the range in voltage from one end of the MAGENTA line to the other amounts to ~ 0.5 MV. Even if that line were extended past 300 kA, the variation in voltage remains at ~ 0.5 MV. The single BLACK diamond point in the plot is the result of an LSP simulation (Paul Ottinger) of the Standard Mode assuming an input total current of 650 kA. For this data point Ic = 190 kA. As the assumed bound current drops below 200 kA, it can be seen that the voltage contours begin to turn upward significantly, and now the voltage uncertainty increases beyond that for which the bound current remains in the 200-300 kA range (**Conclusion #5**). To be sure, whether the bound current is boosted by 10% or not, almost all the data from the 45 Outdoor shots discussed here lie above 220 kA, and thus lie in the 'flat contour' zone.

The plots above and the three Equations 1-3 are based on the analysis of Schumer and Ottinger, which is in turn based upon the original Mendel theory (1979) and subsequent publications. An alternate theory for relating total and bound current in a MITL to an estimated voltage is that of Creedon (1975), known as the *parapotential* theory. Using that theory and equations, a plot of voltage contours and the minimum current line can be drawn in Z_0I_c-Z_0I_a space similar to those shown in Figures 29 to 31, along with the Outdoor Shot data. For comparison purposes, such a plot is shown in Figure 32 (provided by Keith Cartwright), which should be compared to Figure 29 above. While the comparison points to an overall similarity, there are two points to note: 1) whereas in Figure 29, the HERMES data points are clustered to the left of the

minimum current line, in Figure 30 they are observed to straddle the minimum current line, similar to their location in Fig. 30. In Figure 30, the bound current maxima (MK7) are multiplied by 1.1; and 2) whereas the HERMES points in Fig. 29 cluster mostly between the 18 and 19 MV contours, in Fig. 32 they cluster mostly between 19 and 20 MV. In other words, the Creedon model, when compared to the Mendel-Ottinger model, shifts the voltage contour minima to the *left*, and the voltage contours themselves *up*. The difference in estimated voltage is then ~ 1 MV. Based upon anecdotal comparisons of voltage estimates at lower

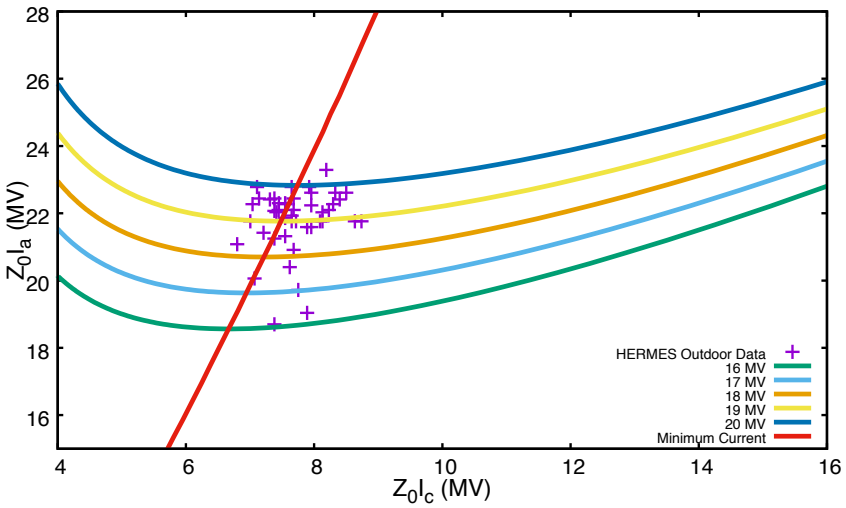

Figure 32

operating voltages, this is a non-trivial amount. The assumptions underlying each model need to be investigated more closely.

The contours in the Ottinger 2006 model are derived from PIC simulations using a generic MITL and electron beam load. A turn-on threshold for electron emission from the inner MITL is set at 300 kV/cm. The Creedon model, by contrast, effectively assumes a *zero* kV/cm emission threshold, since it posits an electron flow that is born somewhere upstream and propagates in the MITL. The HERMES data itself may provide evidence towards an appropriate turn-on threshold. The total and bound current waveforms for Shot 10433 are plotted in Figure 6. Note that the two waveforms are initially equal up to a value of ~ 100 kA. One interpretation is that the MITL has not itself turned on until this level of current is reached. An anecdotal comparison of many HERMES shots indicates that this 100 kA is typical for the value at which the total and bound currents separate. Prior to MITL turn-on, neither Mendel nor Creedon models apply, and the voltage is determined by multiplying either current by the MITL vacuum impedance, which for HERMES is 34 ohms. This ~ 3.4 MV, which when divided by the MITL gap yields ~ 370 kV/cm for an estimated turn-on threshold. The indication then is that, as regards turn-on threshold, that the Mendel model fits the data better than the Creedon model.

More recent LSP simulations have been completed by Paul Ottinger. In the recent simulations, the load region geometry is different from the 2006 simulations, in that the particular HERMES Standard Mode geometry is simulated. In the Ottinger model, the value of g depends upon the assumed MITL turn-on threshold, but in addition, g is affected by the geometry in the load region. As part of the same simulations that yielded the single data point shown in Figures 29 to 31, the MITL turn-on threshold was varied to determine the effect upon the voltage contours shown in Figures 29-31. An example of two plots with, respectively, 200 kV/cm and 600 kV/cm, is shown in Figures 33 and 34. As can be seen, the differences are

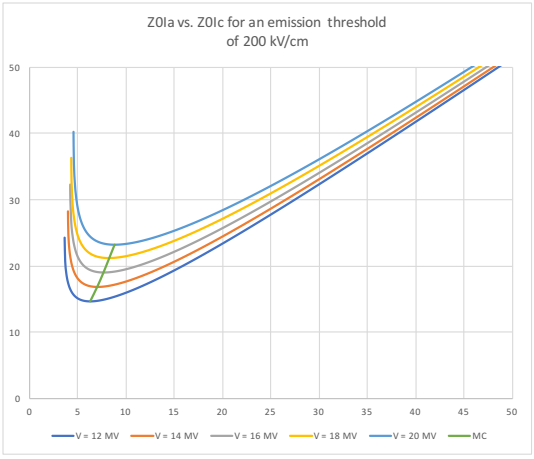

Figure 33

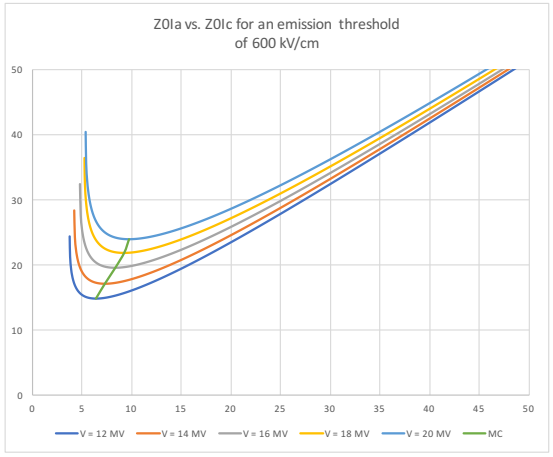

Figure 34

relatively subtle. It can then be inferred that the exact value of the MITL emission threshold has a second-order effect on the simulation results. Comparing the plots with the Creedon data plotted in Figure 30, the magnitudes of the voltage contours are similar, but the minima in the hyperbola curves occurs at a greater z-value. The new LSP voltage contours also appear to be slightly higher than those plotted by use of the equations in the 2006 Ottinger paper (Figures 29-31). Whereas, for example in the contours plotted in Figures 29-31, g = 1.2 at 18 MV, in the two plots above (Figures 33-34), g varies from 1.04 at 18 MV (200 kV/cm) to 1.52 at 18 MV (600 kV/cm).

The major difference between the Creedon and Mendel models can be seen in Figure 35 below, reprinted from the Ottinger 2006 paper. In this plot, only a single voltage contour is plotted, V = 3.94 MV, i.e. significantly lower voltage than the plots above. The different contours are plotted using the different models discussed here. The GREEN curve is Eq. 1 with g = 1, i.e. the Mendel equation. The BLUE curve is the Ottinger modification, with g = 0.843. The BLACK squares are LSP simulation results from 2006, and the RED curve is derived from an earlier version of the Mendel theory. That leaves the BLACK curve, which is derived from Creedon's parapotential model. While the curves come together on the right-hand side ('super-insulated' flow with lower flow levels), they deviate towards the left-hand side, or 'saturated' side of the curves. As has been previously stated, the Creedon model assumes a 0 kV/cm MITL turn-on threshold, e.g. electrons enter the region from outside already born. In addition, the model assumes that the electrons obey laminar flow, e.g. their orbits are all parallel to the inner MITL surface, whereas the Mendel model places no constraints upon the electron trajectories. While a thorough comparison of the Creedon and Mendel models is outside the scope of this Report, there are two observations to make here:

1) The inclusion of this discussion highlights the uncertainties involved in attempting to use MITL theory to estimate voltages in HERMES, and
2) As a practical matter, the inclusion of the BLACK curve in Figure 35 extends the length of the MAGENTA curve in Figure 31. That is, the peak value of the bound current can be varied even beyond the 200-260 kA plotted in that Figure. The lower bound can be extended to below 200 kA, since the upward bend in the voltage contours is pushed towards the left.

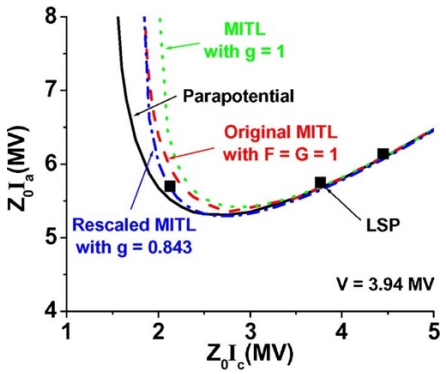

Figure 35

To summarize, while it is of theoretical interest as to whether the HERMES MITL current flow lies closer to the 'super-insulated' or 'saturated' part of Z_oI_c-Z_oI_a space, from the standpoint of voltage determination, the value of the bound current can vary a significant amount and still not affect the resulting voltage uncertainty that much. If one includes the uncertainty in the g factor, the uncertainty in deriving the average currents from the individual IAS1 and MK7 current monitors, and the uncertainty in the 10% 'boost' factor for MK7, the net voltage uncertainty is estimated to lie in the range ± 1 MV, perhaps even ± 0.75 MV. On the other hand, if the IAS1 current is assumed to be 'not dedrooped', the resulting uncertainty is significantly higher, 2 MV or more.

4c. Scaling of the 45-shot TLD data, taking both voltage and current into account.

As was seen in the data review (Section 4a), there is quite a bit of scatter in the current, voltage, and dose data for the 45 Outdoor shots featured for this Report. The scatter is reduced if on any given shot, both the current *and* voltage for that shot are considered at the same time. As already mentioned, the radiation dose-rate from the converter should be expected to scale as IV^x, where I is in Amperes, V is in MV, and x is a factor yet to be determined. It is dependent on a) the angle(s) at which the electrons strike the converter, b) the angle of the dose-rate detector with respect to the converter plane, and c) materials in the path of the photons emitted from the converter. As with the RITS-6 SMP project, all of this information could be input into a ITS-CYLTRAN simulation, and the result would be a predicted x which is a function of the assumed electron angles(s). This has not been done for the dose-rate detectors at HERMES, so we are left with making guesses about the value of x. Before that happens, however, the raw dose-rate data (e.g. the PINBcc and SCDcc waveforms) can be related to the faceplate TLD data, the time-integrated dose measured at the converter. Then the first action is to take the respective PINBcc and SCDcc waveforms and time-integrate them. Of the four SCD waveforms that are typically recorded by DAS for each HERMES shot, it is found that SCDBcc gives the cleanest signal without clipping, as therefore is used as the representative waveform for SCD.

The peak values of PINBcc and SCDBcc for the 45 shots are shown in Figures 36 and 37, respectively. The data points for PINBcc show a level of scatter similar to that of the plots previously shown, but the SCDBcc data are observed to behave differently, dropping significantly in magnitude after some 25 shots. The reason for this can be found by consulting the 'Experiment Details' tab in the HERMES-shot-info (BOOM2). From the beginning of this Outdoor Series (Shot 10268) to Shot 10290, the SCD monitor (which is portable) was deployed at a location 20 cm in front of the converter (z direction), and 40 cm in the 'x' direction (to one side). For Shot 10290, the monitor was moved forward to z = 24 cm. Finally, for Shot 10293, the monitor was moved to x = 50 cm, e.g. further to the side, where it remained for the remainder of the Outdoor Series. It is surprising that such a relatively small move could affect the dose-rate that much.

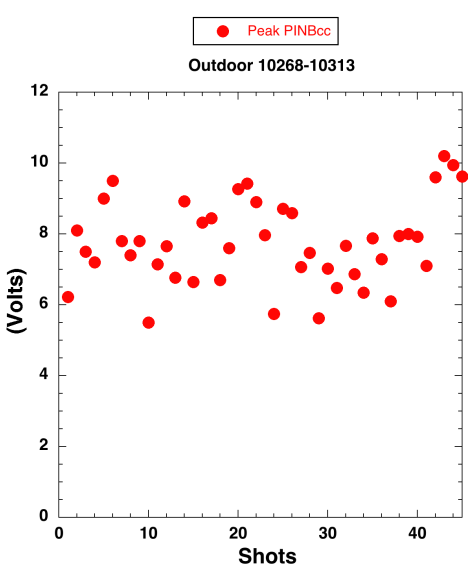

Figure 36. Peak PINBcc

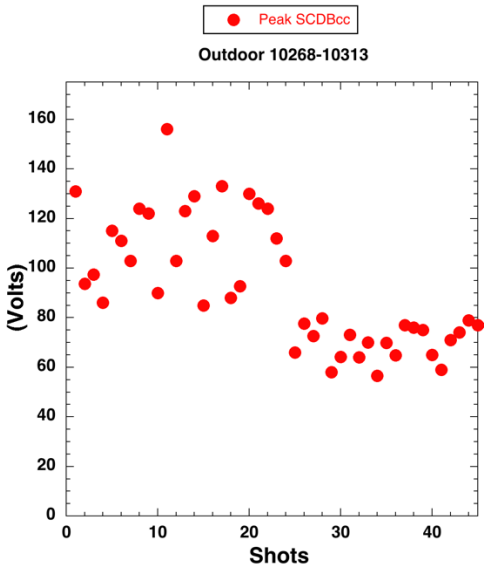

Figure 37. Peak SCDBcc

The PINBcc and SCDBcc signals are time-integrated, and the results shown in (respectively) Figure 38 and 39. As can be seen, the scatter in the time-integrated data resembles that of the peak dose-rate data.

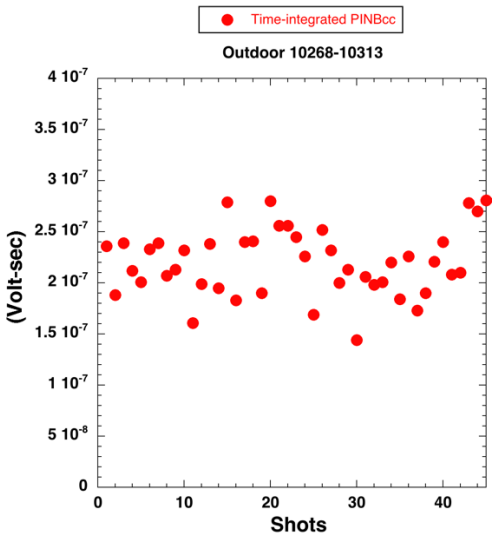

Figure 38. Time-integrated PINBcc

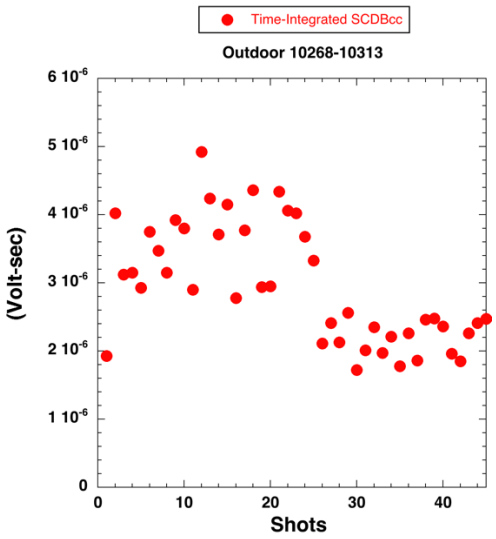

Figure 39. Time-integrated SCDBcc

In the next plots (Figures 40 and 41), TLDSum and dose-area-weighted average (expressed hereafter in Grays or Gy) are, respectively, divided by time-integrated PINBcc. It can be seen that the data scatter is still appreciable, especially when compared to similar plots with time-integrated SCDBcc replacing PINBcc. The latter are plotted in Figures 42 and 43. This means that the SCDBcc dose-rate monitor better tracks the faceplate TLDs when time-integrated, compared to the PINBcc signal, except of course for the ratio change when the SCD monitor was moved. Hence SCDBcc will be used to study the IV^x scaling of voltage and current. That is, the SCDBcc waveform will be scaled to IVx to study the relationship between the two.

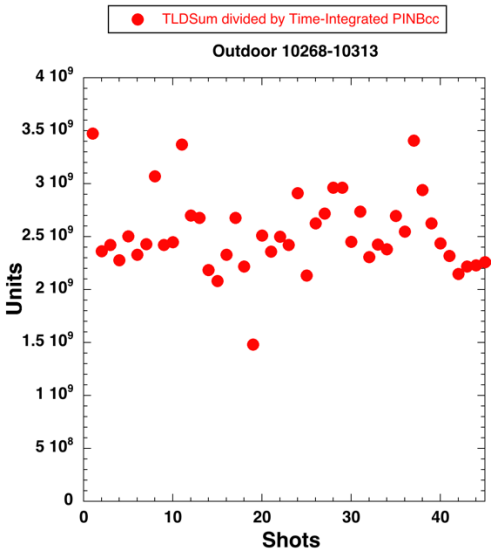

Figure 40

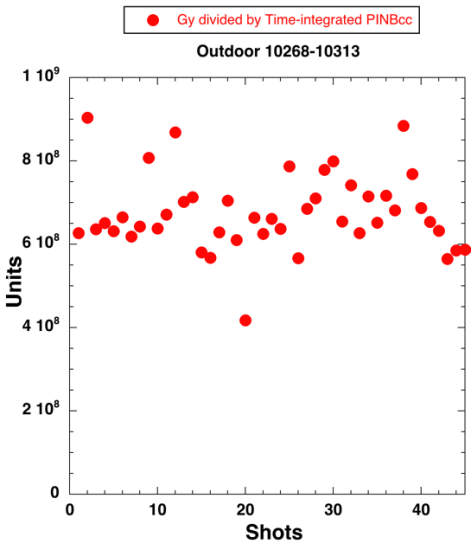

Figure 41

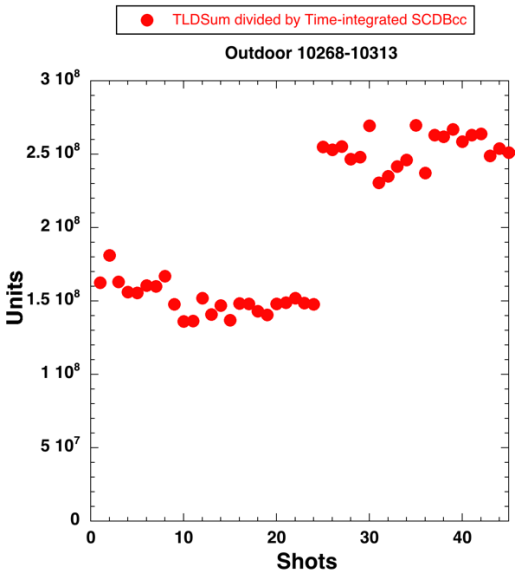

Figure 42

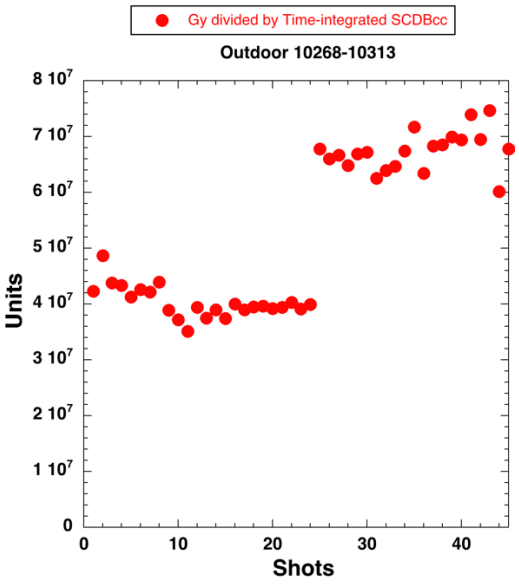

Figure 43

We include here some additional data on the converter current IAS4cc_AVE (new calibration). The fraction of delivered charge at IAS4 (e.g. time-integrated IAS4cc_AVE) as compared to input charge at IAS1 is shown in Figure 44. This ratio is seen to trend downward slightly over the 45 shots, with a fairly constant rate of just under 40% for the last 20 shots in the series. The second plot below (Figure 45) compares the charge delivered to the converter with the time-integrated SCDBcc signal by taking the ratio of the two. The scatter in this data is not as small as that seen with the ratios of TLDSum and Gy to time-integrated SCDBCc seen in Figures 42 and 43 above. This is because the delivered charge (time-integrated IAS4cc_AVE) does not take shot voltage into account. This will be seen in the discussion below Figures 44-45.

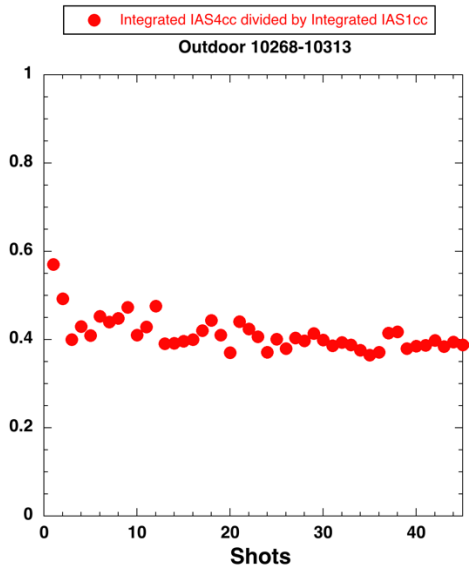

Figure 44

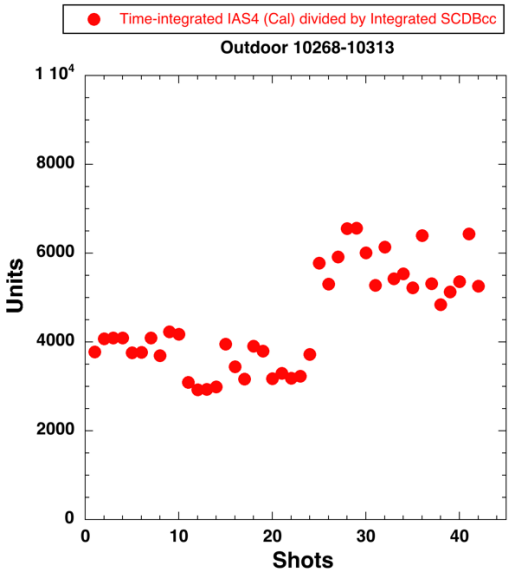

Figure 45

IV^x scaling compared with SCD. In order to take both current and voltage into account, we look at IV^x scaling, as previously mentioned. In the absence of a known value for x, two values are selected for scaling. One is with x = 2.2, and is commonly associated with bremsstrahlung radiation propagated (and measured) in the forward direction with respect to the converter. Another scaling uses x = 1.4, and (from RITS-6 scaling computations) is associated with radiation propagated and measured towards the side, say a 45 degree angle.

To illustrate, the following plot is formed: for each shot, take the Voltage at IAS1 (time-shifted to IAS4 location), in MV, raised to the 1.4 power, multiply by IAS4cc_AVE, and then time-integrate. Then divide this by time-integrated SCDBcc for that shot. The result is shown in Figure 46 below, and the plot should be compared to Figure 45, in which only the time-integrated converter current is used. The data scatter is less in Figure 46, leading to the conclusion that radiation dose is consistent with variations in both voltage and current at the converter. The data in Figure 47 illustrates this also. Here, the dose-area-weighted average (Gy) is divided by time-integrated IAS4cc_AVE, again without voltage input for the shot. The scatter here is much greater, even than in Figure 43 (Gy divided by time-integrated SCDBcc). There is a slight upward trend in Figure 47, reflecting the slight drop in charge at the IAS converter with time.

To show that the scatter in Figure 47 below is not ascribable to fluctuations in the faceplate TLD data (where Gy comes from), we form the following plots: Gy divided by time-integrated IV$^{1.4}$, and Gy divided by time-integrated IV$^{2.2}$, the two variations in x mentioned above. These plots are shown in Figures 48 and 49 below. Unlike the case with Figure 47, the data do not trend upward, but remain relatively flat. The data scatter in Figures 48-49 appear comparable, although it may be argued that the IV2.2 scaling (Figure 49) produces more of a scatter. In any case, the data scatter is sharply reduced from the scatter in the raw Gy data itself (Figure 25). This further reinforces the point that variations in the faceplate TLD data can be explained by variations in the voltage and current reaching the converter.

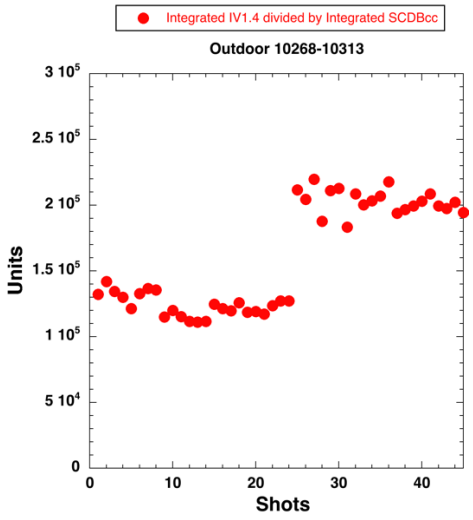

Figure 46

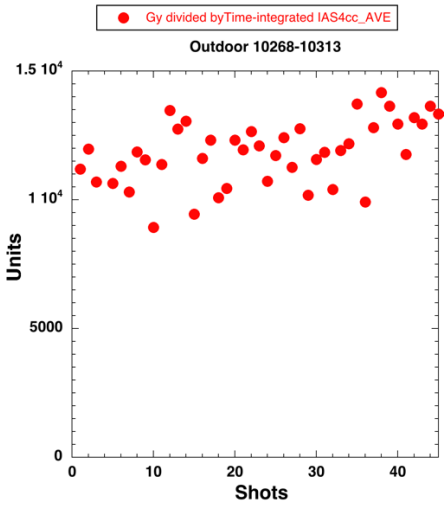

Figure 47

There is a further point to be made here. The same calculation exercise was performed on a Standard Mode dataset (15 shots spread out over time). For this exercise, the Voltage at IAS1 (in MV) was time-shifted 6 ns to the IAS3 position, raised to the 2.2 power, multiplied by IAS3cc_AVE, then time-integrated. The dose-area weighted average (Gy) was calculated from the faceplate TLDs for those Standard Mode shots. The resulting data are plotted in Figure 50. There is quite a bit of scatter in the data, but an informal 'eyeball' of the data suggests an average of ~ 32 units. This should be compared to the same IV2.2-scaled data for the Outdoor Series in Figure 49. A similar 'eyeball' of Figure 47 suggests an average of ~ 37-38 Units. Since the voltage in the outdoor shots is the voltage at IAS1 time-shifted forward, and since there is no observed systematic difference between the voltage at IAS1 between the Standard and Outdoor Mode shots, the only difference in the IV2.2 scaling is with the converter current. The difference between 32 and 37-38 units for the Dose/time-integrated IV2.2 comparison suggests that the calculated IAS4cc_AVE currents resulting from the adjusted gauge factors (short-circuit shots) may be too low by ~ 15%. While 15% may seem like a significant discrepancy, it is much lower than previous calculations of what the dose at the faceplate should be for Outdoor Mode shots (Tim Pointon and Bruce Weber, private conversations). If then the 40% estimate for transferred charge from IAS1 is raised by 15%, this would mean that something like 46% of the total charge is transferred to the Outdoor converter from IAS1. This is still a large loss in current with the use of the Outdoor Mode hardware.

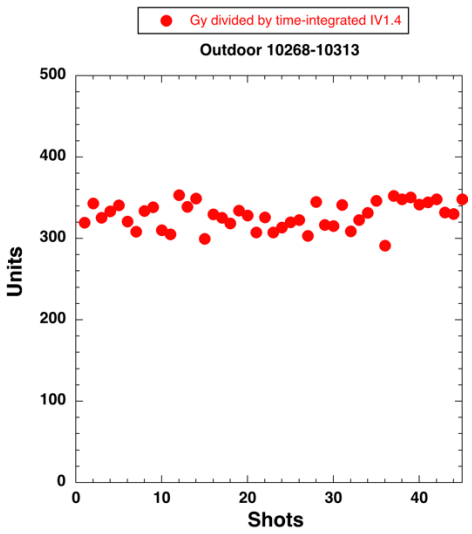

Figure 48

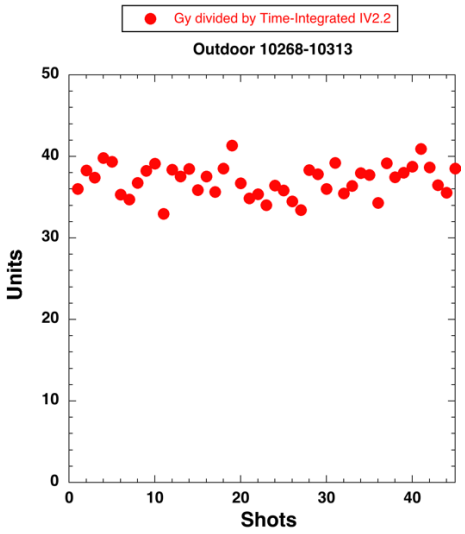

Figure 49

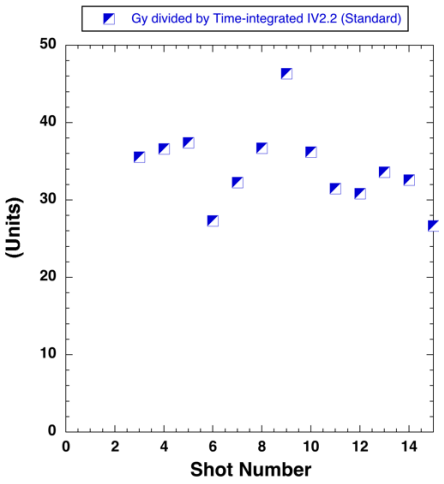

Figure 50

Comparisons of dose-rate waveforms with IV^x. Data comparisons shown above involve time-integrated values for dose-rate monitors, TLDs, and IV^x for various values of x. Here we look at time-resolved comparisons using primarily the SCDBcc monitor. Some limited comparison will be also made with the PINBcc waveform. It is already concluded from Figures 40-43 that there is less correlation with the TLD data using the PINBcc waveform than with the SCDBcc data. It will be shown that some of the dose-rate making up the PINBcc waveform can be ascribed to losses long the MITL that do not appear in the SCDBcc waveform. If so, this would reflect the losses along the MITL that apparently do not contribute to the faceplate TLDs.

We first focus on the one of the Outdoor Shots, 10287. Scalings of IV^x to SCDBcc with various values of 'x' were attempted. The best result was obtained with x = 1.1. For this shot, the z-position is listed in the

'Machine Setup' as 20 cm, while the x-position (e.g. off-axis) is listed as 40 cm, a distance twice as far off-axis as the distance in the axial direction. This amounts to an angle of 63° off the radiation axis. Again comparing to the RITS dataset, x = 1.1 is the power associated with the PIN diode located at 105° (PIN_3 and -5) off the radiation axis. This is significantly different from the 63° angle. On the other hand, it is possible that the 'x' value is symmetric about the 90° position, and that would put the effective observation angle at 85°, somewhat closer to the indicated 63° angle.

To illustrate waveform fit using x = 1.1, the voltage at IAS1 on Shot 10287 (in MV) is raised to the 1.1 power, time-shifted 45.75 ns to the IAS4 location, and multiplied by IAS4cc_AVE. The SCDBcc waveform for the shot is time-shifted +3 ns, and the two resulting waveforms are scaled to Unity and plotted together. This is shown in Figure 51. Separately, the time-shifted voltage is scaled to the peak of IAS4cc_AVE (which peaks at 247 kA), and the two are plotted together in Figure 52.

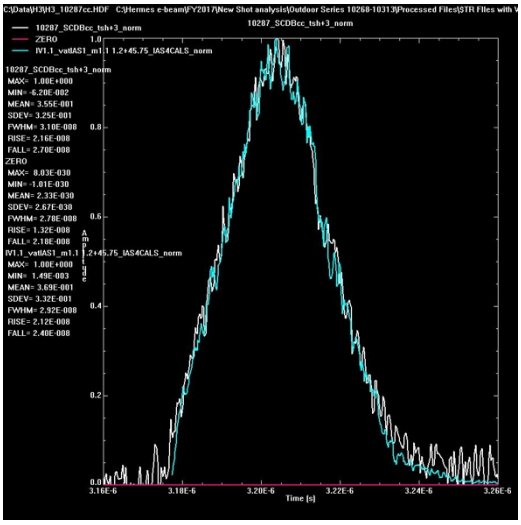

Figure 51 - 10287
WHITE = SCDBcc, BLUE = $IV^{1.1}$

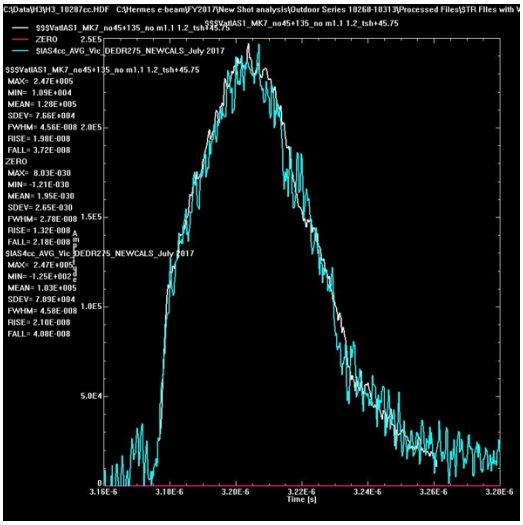

Figure 52 - 10287
WHITE = Vat IAS1+45.75ns, BLUE = IAS4

Several conclusions can be drawn from Figures 51-52:

1) The fit between scaled SCDBcc and IV1.1 for this shot is excellent, and validates the waveshapes of the voltage at IAS and IAS4cc_AVE, if not their magnitude (waveforms are scaled). The SCD monitor appears to describe the radiation field expected at the converter quite well.
2) The shape of the (scaled) voltage at IAS1, timeshifted forward +45.75 ns, fits the shape of the IAS4cc_AVE waveform almost perfectly. This is consistent with the QUICKSILVER simulation result that the voltage at IAS1 proceeds down the MITL in a manner unchanged in waveshape. We can't say whether the peak magnitude is unchanged given the plot in Figure 52, since it is a scaled plot. But the prior discussion concerning $IV^{2.2}$ scaling comparisons between the Standard and Outdoor Modes suggests that the magnitude also remains unchanged as the voltage propagates down the MITL towards the Outdoor converter.

The fit between SCD and IV1.1 for Shot 10287 is in fact typical for most of the Outdoor shots in this Series, with one class of shots as an exception. On Shot 10287, the fraction of charge transferred to the IAS4 position is 0.37. The shots for which there is a good SCD – IV1.1 fit tend to feature a charge transfer ratio of 40% or less. There are selected shots in the Series for which SCD does *not* fit IV1.1. These are correlated

with *larger* than 40% charge transfer. As an example, we consider Shot 10278. Plots equivalent to Figures 51 and 52 for Shot 10287 are shown in Figures 53 and 54 below for Shot 10278.

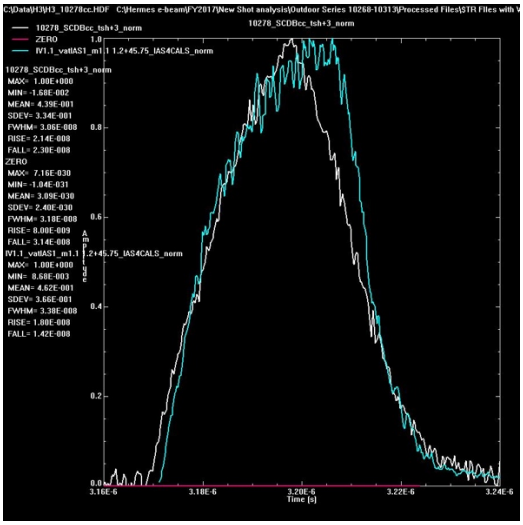

Figure 53 - 10278
WHITE = SCDBcc, BLUE = $IV^{1.1}$

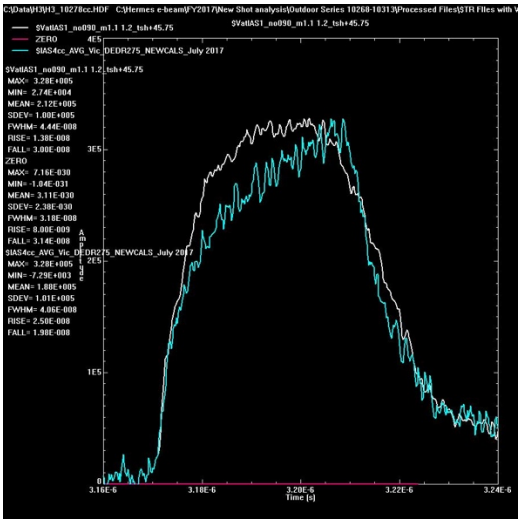

Figure 54 - 10278
WHITE = Vat IAS1+45.75ns, BLUE = IAS4

Figure 53 for Shot 10278 should be compared to the same respective data for Shot 10287 (Figure 51). The SCDBcc waveshape does *not* match the scaled IV1.1 waveform for the Shot, as the latter peaks much later in the pulse. Similar comparisons of Figures 52 and 54 show that on Shot 10278, the time-shifted voltage at IAS1 (scaled) does not fit the averaged IAS4cc current. For Shot 10287, the transferred charge fraction to the converter is 37%, whereas for Shot 10278, the number is almost 48%, a significantly higher amount. This appears to be an anecdotally consistent observation, that higher charge transfer fractions are associated with a IAS4cc_AVE waveform that is shaped differently from the voltage at IAS1 waveform. The higher charge transfer fraction occurs on a minority of shots, but appears always corelated with the V at IAS1 – IAS4 mismatch in waveshape.

This enhanced peak value for transmitted current to IAS4 on Shot 10278 is in fact associated with an asymmetry on the faceplate TLD response on that shot. Referring now to Figure 23, which gives the layout of the 29 faceplate TLDs, the values for the locations 3 and 5 (e.g. either horizontal side of the center TLD) are, respectively, 45.87 and 41.89 krads. In addition. TLD #8 (northwest of center) features an abnormally high reading (42.9 krads). The 3 respective readings for Shot 10287 are: 26.56 krads, 25.65 krads, and 20.01 krads. This clearly suggests that the beam current is higher on Shot 10278, and with a beam centroid located off-center and to the left, relative to the faceplate TLD readings.

At this point, it is not known why the increase in transmitted current/charge to the Outdoor converter is correlated with changes in waveshape to the IAS4cc_AVE signal. Further insights could possibly be gained by analyzing a more complete set of TLDs arrayed along the MITL, instead of just the faceplate TLDs. In addition, absolute calibration of the dose-rate monitors (by fielding accompanying TLDs at each monitor location), as well as a comprehensive ITS-CYLTRAN modeling of the dose-rates would be quite helpful. In the absence of this, we point out some dose-rate – IVx correlations of anecdotal interest, and leave any further investigations to future work.

Additional IV^x – dose-rate comparisons. The excellent correlation between IV1.1 and (scaled) SCDBcc seen on Shot 10287 (Figure 51) is repeated quite often in the 45-shot Series discussed here. For example, we plot similar waveforms for Shot 10276. The comparison between IV1.1 and SCDBcc is shown in Fig. 55. This shot is chosen because, in addition to the overall excellent fit, there is a waveform feature – a 'pause' on the rise – that is captured in both waveforms. The reason for this pause is suggested in Figure 56, which compares the time-shifted voltage at IAS1 (scaled) to IAS4cc_AVE. On the latter waveform (BLUE), there is a pause near the peak, and then a quick jump in the waveform shape to its peak. This jump in current – without an accompanying jump in the voltage – appears to be the reason for the 'pause' feature in Figure 55.

The waveforms plotted in Figure 57 below have not been previously discussed. The WHITE curve is (scaled) PINBcc for Shot 10276. The BLUE curve is IVx, where now x = 1.8 instead of 1.1. (PINBcc is time-shifted +8 ns for this plot.) That is, the PINBcc waveform shapes I judged to be narrower in FWHM than SCDBcc, and so requires an increased value for x. Here, the pulsewidth is correctly captured, as well as the back half of the comparison, but not the front half. Still, while the waveform match is not good for the front half, the shape has some similarities, which bears further investigation.

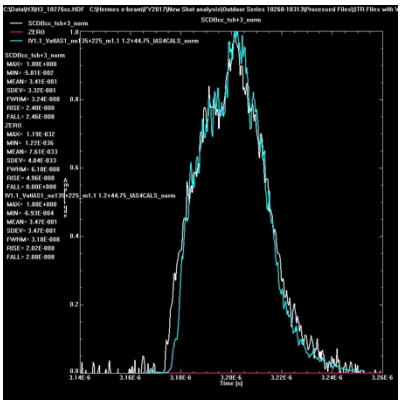

Figure 55 - 10276
WHITE = SCDBcc, BLUE = IV$^{1.1}$

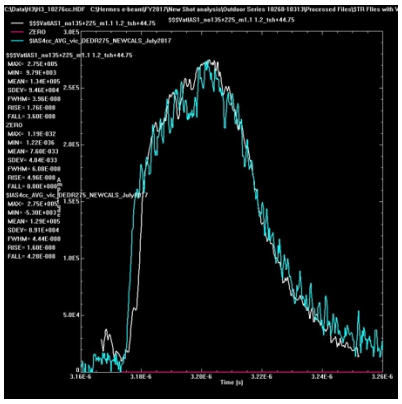

Figure 56 - 10276
WHITE = Vat IAS1+44.75ns, BLUE = IAS4

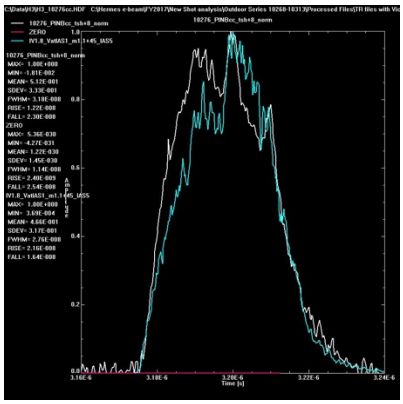

Figure 57 - 10278
WHITE = PINBcc, BLUE = IV$^{1.8}$

Shot 10301 is another shot in the Outdoor Series under discussion. A plot similar to that in Figure 57 is shown in Figure 58 below. That is, the WHITE curve is PINBcc (+8 ns) for Shot 10301, and the BLUE curve is IV1.8. Here, the back half of PINBcc follows the scaled IV1.8 waveform almost exactly. To investigate this further, we plot the PINBcc and SCDBcc waveforms (scaled) *together*, instead of compared to IVx. This is shown in Figure 59. The scaling chosen is of heuristic interest. While the back half of both waveforms track each other well, the front half of PINBcc exceeds that of SCDBcc, in a way that suggests that PINBcc is enhanced compared to SCDBcc early in the power pulse. For Figure 60, the two waveforms in Figure 59 are subtracted – that is, SCDBcc in the plot is subtracted from PINBcc. The difference (WHITE) is then scaled upward, and plotted against the XMB4090cc waveform (uncalibrated – upstream of IAS4) in RED, and the IAS4cc_AVE waveform (BLUE). The shape of the difference suggests current loss along the MITL, in a form that is detectable by PINB but not SCDBcc. Recall that the PINBcc monitor is located more off-axis to the Outdoor MITL, whereas the SCD monitor is located closer to the converter location, and hence may not be in a position to detect the losses along the MITL.

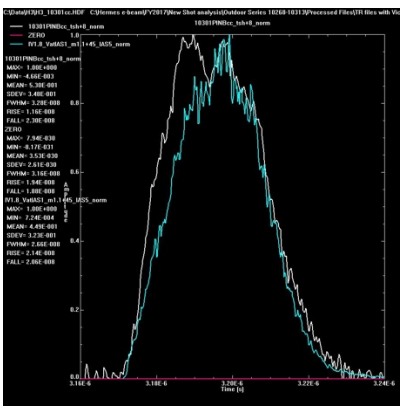

Figure 58 - 10301
WHITE = PINBcc, BLUE = IV1.8

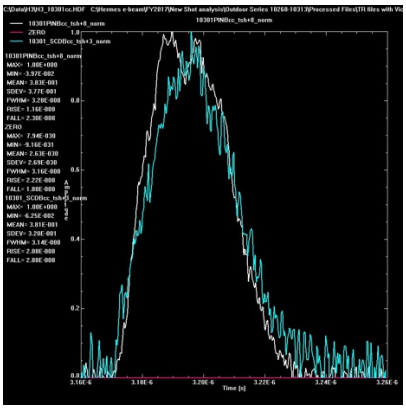

Figure 59 - 10301
WHITE = PINBcc, BLUE = SCDBcc

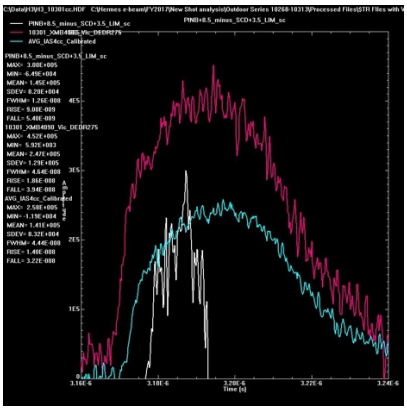

Figure 60 - 10301
WT= PINB-SCD, RD=XMB4090, BLU = IAS4

There *is* an alternative explanation for the difference between the PINBcc and SCDBcc waveshapes. This is illustrated by looking at data from Shot 10271. The equivalent plot to Figure 58 is shown in Figure 61, i.e. PINBcc (scaled) is plotted with IV1.8 for the Shot. Compared to the Shot 10301 data, the PINBcc waveform (and the IV1.8 as well) has a complicated structure, but there is an interesting parallel between the two waveforms. This is illustrated by the plots in Figure 62, which require some explanation. In the Figure, the WHITE waveform is the same as the BLUE waveform in Figure 57, i.e. scaled IV1.8. There are in addition to the WHITE signal, *six* individual pieces that when spliced together, make up an alternative waveform that follows the WHITE signal quite well. These six pieces are created by a) slicing the PINBcc waveform into six individual pieces, and b) for each piece, scaling to the WHITE by multiplying by a different factor. The first piece (OFF-WHITE) is formed by cutting off the PINBcc signal at 3.187 µsec, normalizing, then multiplying by an additional factor 0.79. The second piece (RED) takes PINBcc only between t = 3.187 and 3.194 µsec, and multiplying by 0.91 instead of 0.79. The third piece (MAGENTA) uses the following numbers: 3.194 to 3.200 µsec, factor 1.0. The fourth piece (DARK BLUE): 3.200 to 3.205 µsec, factor 1.07. Fifth piece (LIGHT BLUE): 3.205-3.209 µsec, factor 1.15. And finally, the sixth piece: after 3.209 µsec, factor 1.27.

Note that each of these time slices amounts to ~ 5-6 nsec, except for the first and last slices. And in each succeeding slice, the multiplicative factor needed to match the IV1.8 waveform increases. Mathematically, the same waveform fitting could be accomplished by modifying the 'x' in IV^x, but not in a random manner, but a systematic one. In this case, then unlike all the previous IV^x waveform plottings above, the 'x' is longer fixed, but it changes (specifically, increases). This implies that, from the standpoint of the PINBcc monitor, the Radiographer's Unfold only works if the x-factor changes. From previous RITS-6 analyses of SMP diode experiments, this implies that the electron-beam pinch angle to the converter is changing. But as we have seen, the IV1.1-SCDBcc fit is excellent on most of the 45 shots discussed here. In these plots, the 'x' is 1.1, and it does NOT change. So one monitor analysis suggests that the electron pinch angle changes, the other does not.

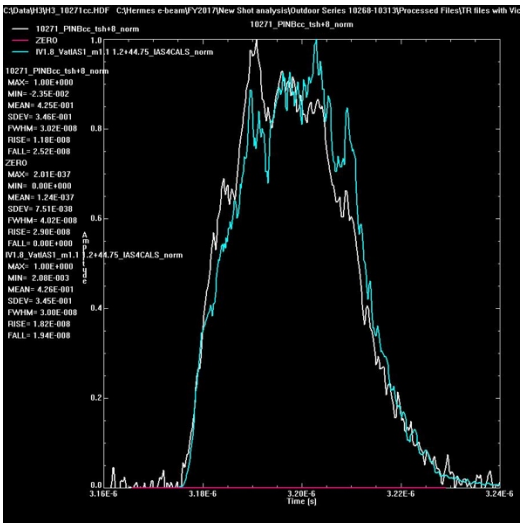

Figure 61 - 10271
WHITE = PINBcc, BLUE = $IV^{1.8}$

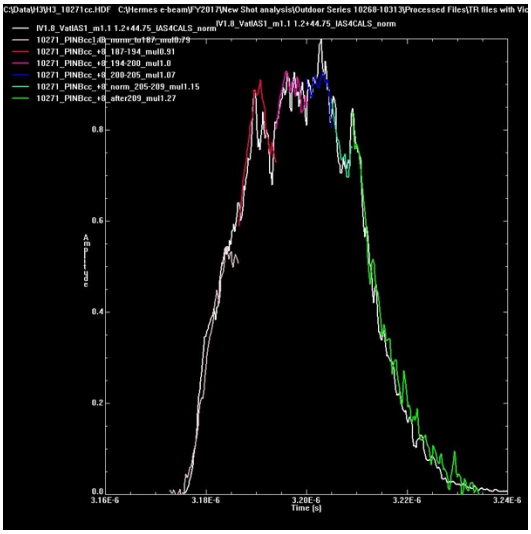

Figure 62 - 10271
WHITE = $IV^{1.8}$, Multicolor = PINB (Scaled)

There are several possible explanations for this seeming discrepancy:

1) The mathematical modification to the Shot 10271 PINBcc waveform (Figure 62) is purely coincidental. This seems possible but unlikely.
2) SCDBcc and PINBcc are, respectively, located at viewing geometries for which the inferred pinch angle does *not* change for SCDBcc, but *does* change for PINBcc. While improbable, this is not impossible to imagine, but requires the full absolute calibration and ITS-CYLTRAN unfold modeling similar to that already accomplished with RITS-6 SMP data.

In the absence of further modeling work, we cannot conclude whether the discrepancy between the SCD and PINB signals is caused by selective loss observation, and changes to electron pinch angle. This would be a subject for future work.

5. ADDENDUM. BRIEF COMPARISON WITH OUTDOOR SERIES 10639-10711.

This is a later Outdoor shots series than the subject of this Report. Two observations are worth noting:

1) **Scaling of IV^x with SCD**. In the previous discussion of the present Outdoor test series, it was pointed out that the best fit to the SCD waveform occurred with x = 1.1. In the later test series, the optimum fit occurred with the 'x' raised to 1.8. The reason has to do with the placement of the (portable) SCD monitor. The angle of placement for the current series was at least 63° off the radiation axis. For the newer test series, the placement was with the z and x coordinates almost equal, e.g. the angle of placement was approximately 45°. Again recalling the RITS-6 database, this angle was approximately the same as for the PIN_6 monitor in that experiment. The x-scaling for PIN_6 was 1.8. This suggests that the scaling with observation angles observed on RITS has more universal application than for just the RITS shot series.

2) **Absolute dose**-rate. For the newer shot series, tag-along TLDs were fielded with the PINB, SCD, and SCDREF monitors, with the intent of determining absolute dose-rates in krad/sec. The full data summary is available in the 10639 – 10711 Shot Summary (separate), but in brief, the absolute dose-rate associated with the PINB monitor more closely tracked the faceplate TLDs than the raw dose-rate itself. This was not the case with either the SCD or SCDREF monitors. This suggests that the position of the tag-along TLD was in a good location for the PINB monitor, but not for the other two monitors. This also suggests that future experimentation with optimizing those tag-along TLD locations may result in a reliable dose-rate location for those two monitors.

REFERENCES

1. Gerald Zawadzkas, *The Hermes-III Gamma-Ray Facility at the Simulation Technology Laboratory – A Guide for Users, Sandia Report SAND89-081 – UC-02, Printed April 1989.*

2. Thomas W. L. Sanford, *History of HERMES III Diode to Z-Pinch Breakthrough and Beyond*, Sandia Report SAND2013 – 2481, Printed April 2013.

3. P. F. Ottinger and J. W. Schumer, *Rescaling of equilibrium magnetically insulated flow theory based on results from particle-in-cell simulations,* Phys. Plasmas **13** (2006), 063109-1 - 063109-17.

4. C. W. Mendel, J. Appl. Phys. **50** (1979) 3830.

5. John M. Creedon, *Relativistic Brillouin flow in the high v/γ diode*, J. Appl. Phys. **46** (1975) 2946.

APPENDIX 1: RADIAL TLD MAPS, AND THEIR USE IN DETERMINING ELECTRON ORBITS TO THE CONVERTER

On each of the HERMES shots taken, whether the Mode be Standard, Extended, or Outdoor, an array of TLDS, 29 in all, is fielded in a Radial pattern ('Faceplate TLDs'). The TLDs constituting this 'Radial TLD Map' are mounted on a plate, which is then attached to the end vacuum plate on HERMES. Thus, the individual TLDs are surrounded by metal. At each discrete radius (6,8,12,14,18,20, and 24 cm), there are 4 TLDs mounted in various directions. With the center TLD included, this totals 29 TLDS. This array has been consistently fielded in this manner since Shot 9855, a total of over 800 shots, giving one of the most reliable datasets on HERMES. Accordingly, the Radial Maps and their interpretation are a key component of shot analysis.

In this paper, we interpret the 29 TLDs in two different ways: 1) the TLD doses are simply added together. This total is known as TLD Sum, and is recorded on every shot and listed on the 1342 Sharepoint site under 'Filmmaker Pro Databases'; and 2) The TLD doses are weighted by the area of the annulus in which they are mounted. For each annular ring occupied by the TLDs, the area is approximately $2\pi r\Delta r$, an area which increases as the radius. Dose-area weighting is meant to account for this. There are various ways to perform this weighting. This paper adopts the weighting procedure devised by Bruce Weber of the Naval Research Laboratory, and set up within an Excel spreadsheet, and uses the 'Trapezoidal Rule' to process the 29 TLDs. For each shot, a plot is generated within Excel of the doses as a function of radius. At each radius, the 4 doses are plotted by angle, and then an average is drawn between the points at each radius. Unlike the TLD Sum numbers, the dose is given in Grays (10 Grays = 1 krad). The different unit is used here simply to distinguish the TDLSum and dose-area-weighted datasets. The dose-area average is then the weighted total divided by the total area.

It should be noted that it is not obvious that these two different ways of weighting the TLD doses should yield similar results. For instance, in the case of the dose-area average, the TLD dose at the center is not counted at all, the reason being that its effective area is zero. In the case of TLD Sum, the center TLD is counted just like the others. The difference should be especially noticeable for center-peaked TLD arrays, since the center TLD can contribute up to 15% of the TLD Sum total.

The effect of weighting the center TLD on the dose-area average was tested as follows: an arbitrary radius was mathematically assigned to the center TLD, in stages. The radius was set to 1 cm, then 2 cm, then 3 cm. A radius of 3 cm corresponds to a distance halfway to the first set of radial TLDs out from the center, and should be considered an extreme accommodation for the center TLD weighting in the dose-area average. Nonetheless, a radial assignment of 3 cm changed the dose-area average by only 5%. Intuitively, the reason that the center TLD should be assigned little or no area weighting is even using a 3cm radius, the effective area, compared to the other annular rings, is just not that big. The data comparisons discussed in the main text indicate that either weighting method (TLDSum value or dose-area weighting) produces comparable results. This is, however, only the case when the Radial *profile* of the shots being compared is similar, as is the case with the Outdoor shots discussed here. But if the shots being compared have, for example, peaked-in-center and flat-centered profiles, then the two methods give differing results.

Another parameter that is monitored in the HERMES database is the *average* TLD reading. This is calculated by taking the TLDSum value, and dividing by 29 (the total number of TLDs). The average TLD reading is a parameter that can be directly compared to the dose-area weighted average for a given shot. For illustrative purposes, both numbers are calculated for a recent HERMES shot (10742, Standard Mode). The radial dose profiles from both the dose-area weighting method, and the standard plot shown on the HERMES Shot Summary, are shown (respectively) in Figures 63 and 64. The profiles appear very similar

in shape. For this shot, the average TLD dose is 37.3 krads, whereas the dose-area weighted average is 29.6 krads. The dose-area weighted approach thus de-emphasizes the inner (large) valued TLD readings.

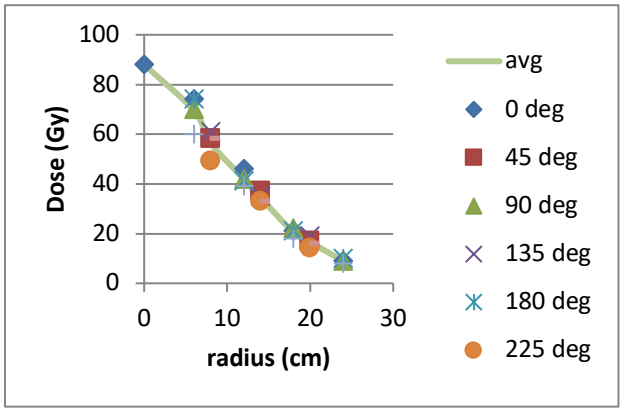

Figure 63 - 10742

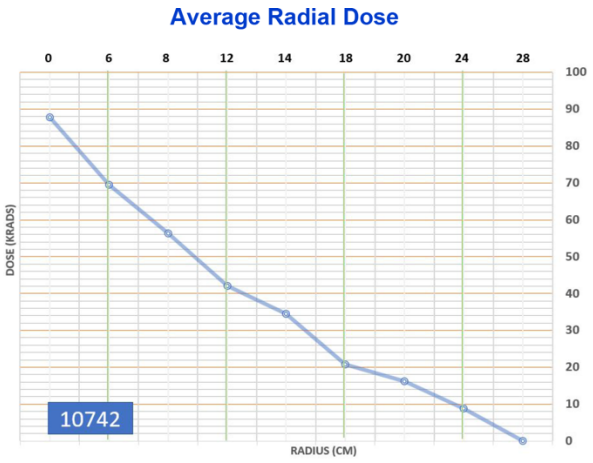

Figure 64

Using the radial layout format of the dose-area weighting method (Figure 63), we can show the evolution of the TLD profiles from the non-center-peaked that was typical before ~ Shot 10240 to the present center-peaked profile. We start with an even earlier Outdoor test series, Shots 10196 to 10223. Since the test series highlighted in this Report (10266 – 10313) occurred after the graphite plug began to be routinely fielded, the total shot span here (10196 – 10313) covers the before-and-after the graphite plug fielding began.

It may be recalled that the purpose of the carbon beam plug is to protect the center of the Ta converter from being damaged by the electron beam. This has occurred in recent times for all Modes, and while the cause has not been well understood, one possibility is the tendency of the HERMES power coming forward to increase with time. This may result in more extensive ion emission from the titanium cover sheet, which in term would cause the electron beam to pinch more readily towards the center of the converter. The first TLD pattern below is taken from Shot 10196, from the first Outdoor Test series. The pattern indicates a 'depressed center' TLD pattern, with a total dose-area weighting of 159 Grays. This type of pattern used to be the normal pattern expected for both Standard and Outdoor Modes. (The Extended Mode typically shows

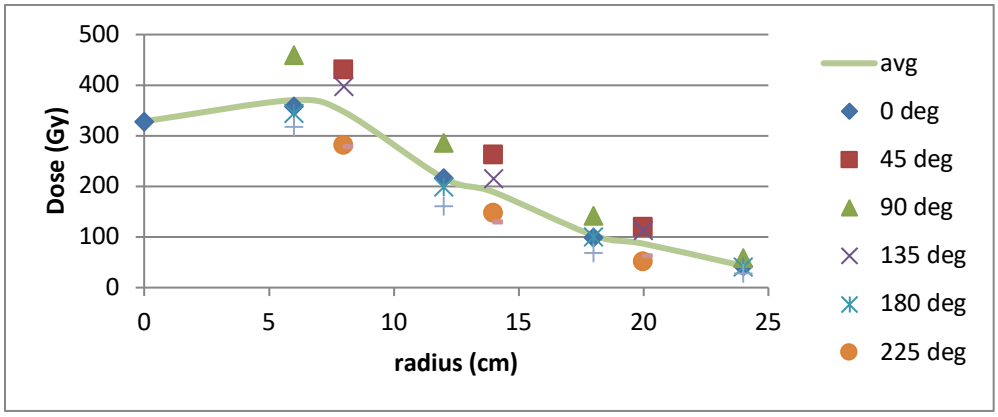

Figure 65. Shot 10196: Dose-area weighted average 159 Grays

a center peak in the TLD array, due to the use of the Trumpet cathode and enhanced current at the converter, compared to the Outdoor Mode.)

The pattern of TLD doses represented by Shot 10196 above persisted through Shot 10199, then became more peaked on axis, as represented by Shot 10201 below.

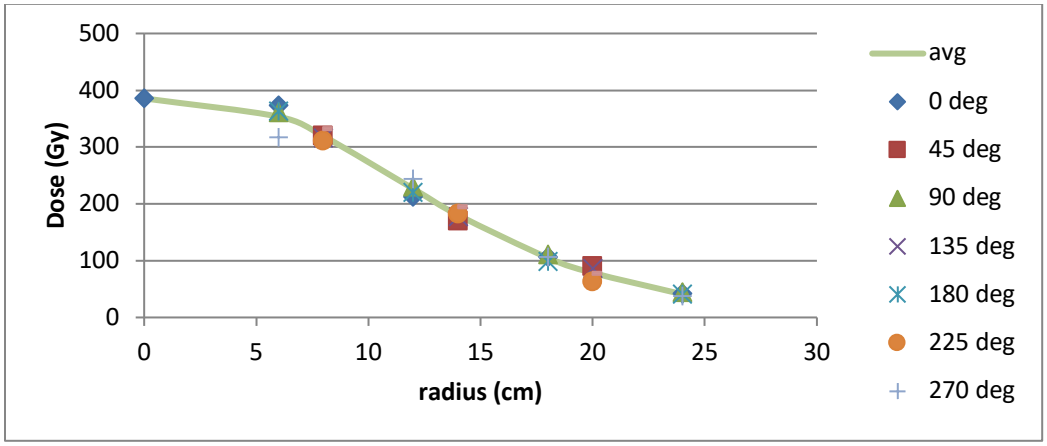

Figure 66. Shot 10201: Dose-area weighted average 154 Grays

This peaked-on-axis pattern persisted for only two shots, however, and the hollow-on-axis or plateaued-on-axis resumed with Shot 10204, and persisted for the remainder of the Shot series, through Shot 10226.

In between the end of this shot series, and the 10268-10313 Shot Series, the graphite beam block became routinely fielded, with the center of the block in contact with the converter package. The pattern of TLD doses began to change. The patterns for the first and second data shots in the Series, Shot 10268 and 10269, are shown in Figures 67 and 68 (next page):

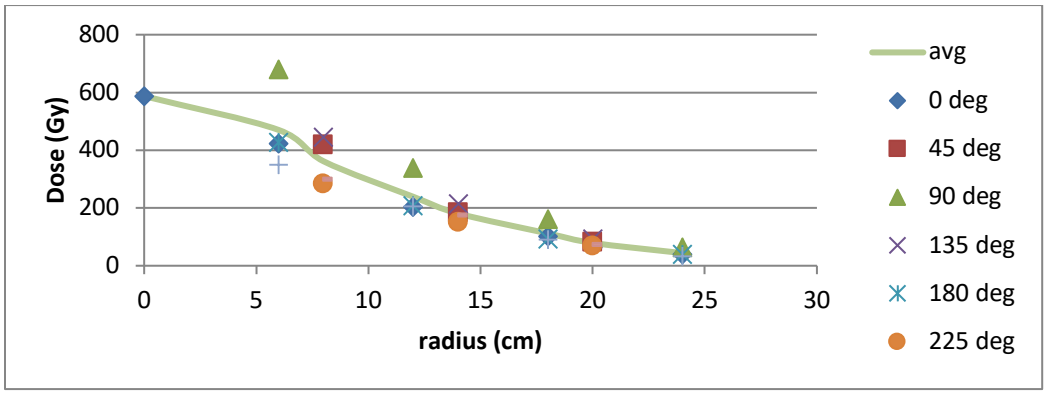

Figure 67. Shot 10268: Dose-area weighted average 170 Grays

The pattern for Shot 10269 shows the most obvious dose peaking at the center. This cannot be ascribed to a stronger e-beam on the converter, since the dose-area weighted average is the lowest of the four shots shown above. Most of the shots up to Shot 10313 have patterns that look similar to Shot 10268, including Shot 10282, which had the lowest dose-area weighted average at 104 Grays.

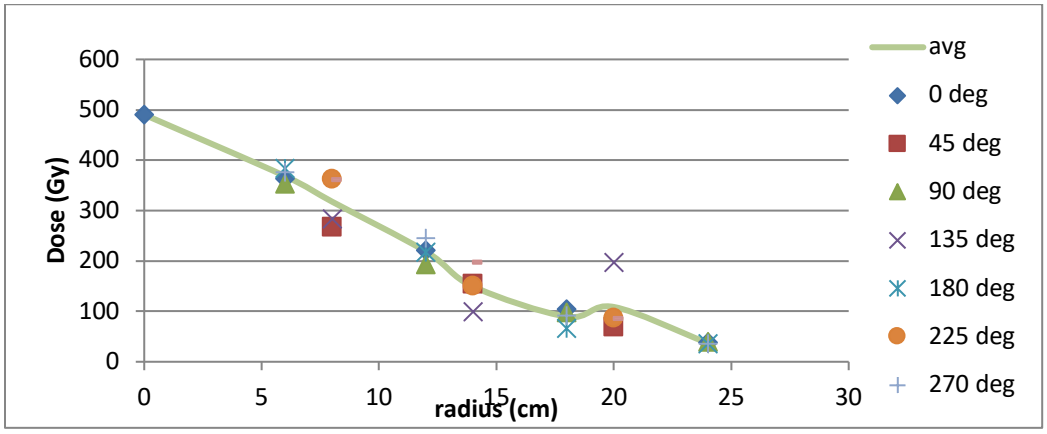

Figure 68. Shot 10269: Dose-area weighted average 152 Grays

The evolution in the TLD radial pattern, from non-center- to center-peaked, has not been well-understood, as already mentioned. Whatever the mechanism, the effect would be to cause either a) the electron *angles* to change on the converter, or 2) the electron *positions* to change on the converter, e.g. the point of impact, or c) both. To help lend insight to the electron dynamics on the converter, MCNP simulations were conducted by Russell Durrer (1342). Unlike the case with LSP simulations, MCNP does not predict the electron distribution self-consistently on the converter. Rather, some assumed input distribution must be assumed. The distributions assumed in the MCNP simulations can be explained by referring to the MCNP setup geometry shown in Figure 69. In this drawing, the graphite plug (1 inch thick by 10 inches in diameter) is centered on the converter facing the electron beam, with the TLD array indicated on the opposite side (open to atmosphere). Two diagonal lines are indicated, marked A and B. Both lines intersect the converter plane at a 30° angle. Two sets of simulations were done. One (Line A) assumes that the electron population intersects the graphite converter at a location 5 inches from the axis, and at a 30° angle. The voltage and current level of the impacting electrons was determined by a representative shot in the series featured in this Report. The other set of simulations (Line B) assume that the electrons strike the converter at the outer edge of the graphite plug, where the plug faces against the converter assembly. In this set of simulations, the angle of incidence was varied, from 25° to 45°.

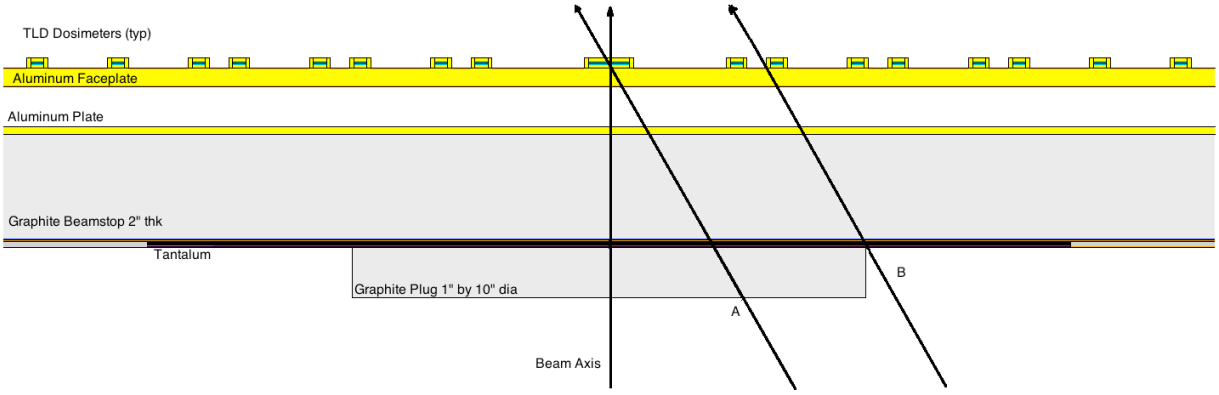

Figure 69. HERMES converter region with graphite plug in place.

One of the key differences between the Line A and Line B simulations is that the Line B results are unaffected by the presence of the graphite plug. An additional simulation was added to Line A: the graphite plug was removed, and results compared to those where the plug was in place. The underlying assumption behind the Line A simulations is that the electron beam has pinched in such that the impact point on the converter (and the graphite plug) is a ring 5 inches in diameter. By contrast, the Line B simulations are meant to model the case where the incoming electrons remain at large enough radius to avoid impacting the graphite plug. The graphite plug is approximately a half-range thick for 18 MeV electrons, so that transmission through the graphite would have a large impact on the resulting dose. A typical electron would then expend half its energy transiting through low-Z material, followed by considerable reduced photon yield upon striking the tantalum converter at half its initial energy.

A plot of TLD radial profiles generated by 4 HERMES shots, with (2) and without (2) the graphite plug in place, is shown in Fig. 70. One of these (10028) clearly exhibits a non-centered peak profile, whereas the other 3 are center-peaked. The remaining non-graphite plug shot (10247) is tracked closely in profile by the two shots with graphite plugs (10433 and 10525). It is clear then that the presence of the graphite plug has a minimal effect on the resulting TLD radial profile.

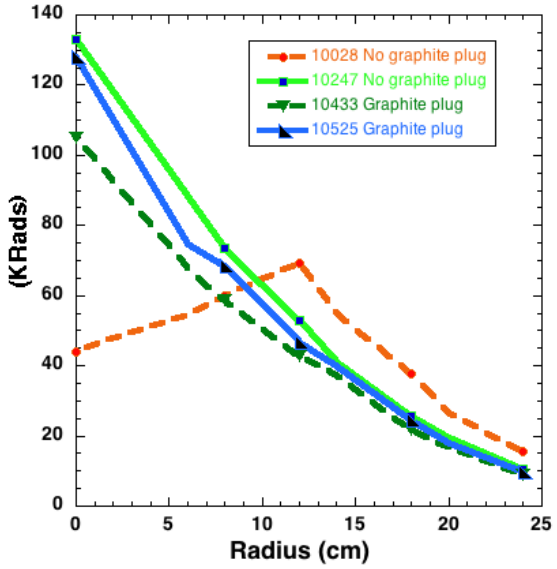

Figure 70. TLD radial profiles w/ and w/o graphite plug

Results from the Line A MCNP simulation (5 inch beam spot, 30° electron angle) are shown in Figure 71 below. The RED curve is the TLD radial array profile from Shot 10547, a Standard Mode shot. The BLUE curve is the predicted TLD output for a 5 inch beam spot where the graphite beam block is kept in position. The graphite is then removed to yield the GREEN curve. Both simulation curves bear no relation to the experimental data, being much larger in magnitude and much more highly peaked about the centerline. The peak of the GREEN curve is left off the plot, because to include it would reduce the experimental data to almost zero on the plot.

Line B simulation results (10 inch beam spot, various electron angles) are shown in Figure 72 below. The effect of increasing the electron angle on the converter from 25 to 35 to 45° is shown by, respectively, the GREEN, BLACK, and RED curves. The evident effect of changing the incoming electron angle is to 'fill in' the dip in the dose at the center. But in addition, the peak predicted dose at the center is drastically

reduced compared to the Line A simulation, and more in line with measured dose profiles. Qualitatively, tilting the electron strike angle in this increasing way replicates what has happened to the experimental TLD radial profiles, e.g. they have steepened from the BLACK curve to the RED curve. Note that the *position* of the electron strikes on the converter has not changed, only their *angle*.

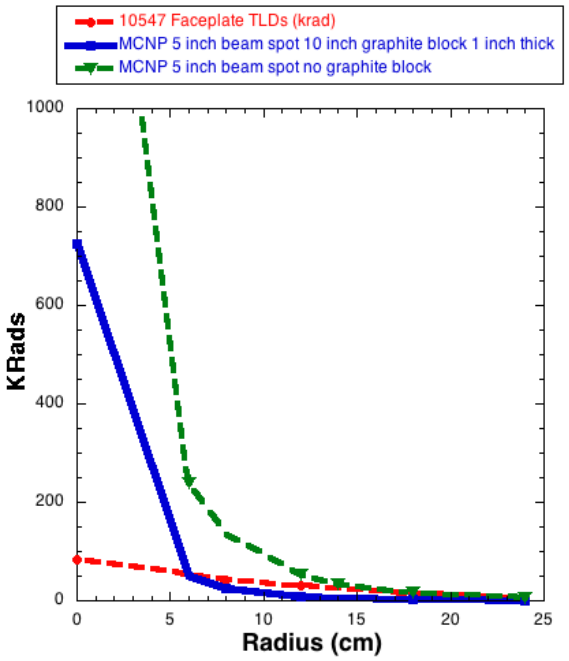

Figure 71 – 5 inch beam spot

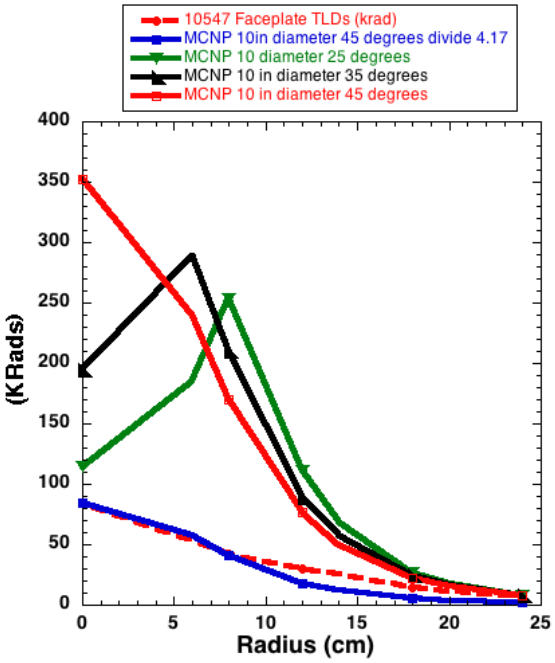

Figure 72 – 10 inch beam spot

There are two additional curves in Figure 72. The DOTTED RED curve is the 10547 TLD radial profile, already plotted in Figure 71. The BLUE curve is the RED curve divided by 4.17. i.e. scaled downward so that the peak of the curve matches that of Shot 10547. The radial shape of the rescaled curve (45° electron strike) closely matches the experimental data.

The following conclusions can thus be drawn from the Line A and Line B simulations: 1) the posited beam impact point of 10 inch diameter (LINE B) can be made to closely match both the general shape of the TLD radial profile, and the evolution of this shape from non-centered peak to center-peak, by simply changing the impact angle from 35 to 45 degrees; and 2) the predictions of the Line A simulations bear no relationship to the experimental data, being far too high and far too peaked on center. The conclusion from the MCNP simulations is that on HERMES shots, ***whether the graphite plug is in place or not, is that the beam electrons remain at a radius > 10 inches in diameter, e.g. they do not impact the graphite, at least during the radiation-generating part of the power pulse.***

There is HERMES experimental data that supports this conclusion. One of the diagnostics fielded on selected HERMES shots is an x-ray pinhole camera. The camera, heavily shielded due to the extreme x-ray environment, is fielded either on-axis directly in front of the HERMES diode region, or off at an angle to the radiation axis. An example of the image obtained from the pinhole camera is shown in Figure 73

below, and was taken on Shot 10436, a Standard Mode full-power shot. On the left side of the Figure is the pinhole image. The yellow lines demarcate an area spanning the central part of the image that was

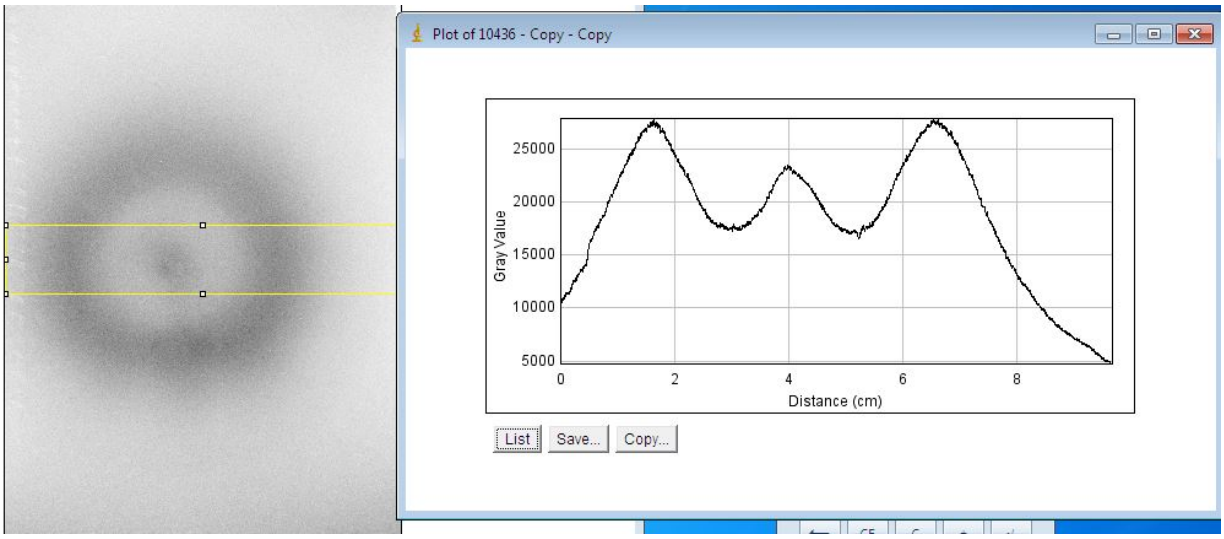

Figure 73. (left) Shot 10436, x-ray pinhole image, (right) densitometer scan

measured by a densitometer (scan at right). The intensity profile is observed to be annular in shape, with lower-level 'hot spot' in the center. The hot spot is predicted by QUICKSILVER simulations, and is due to electron emission from the inner edge of the annular cathode. The emitted electrons converge at a steep angle to the center of the converter. The total number of such electrons is not that high, but the electrons are concentrated over a relatively small area.

The scale shown is of the raw image, which must be adjusted for the magnification factor. The result is that the center of the outer ring is approximately 12 inches in diameter. The diameter of the inner (cathode) MITL is 14.5 inches. Thus, the electron beam is observed to pinch slightly inward, but impact the converter at a diameter that is greater than the diameter of the graphite plug (10 inches). The faceplate

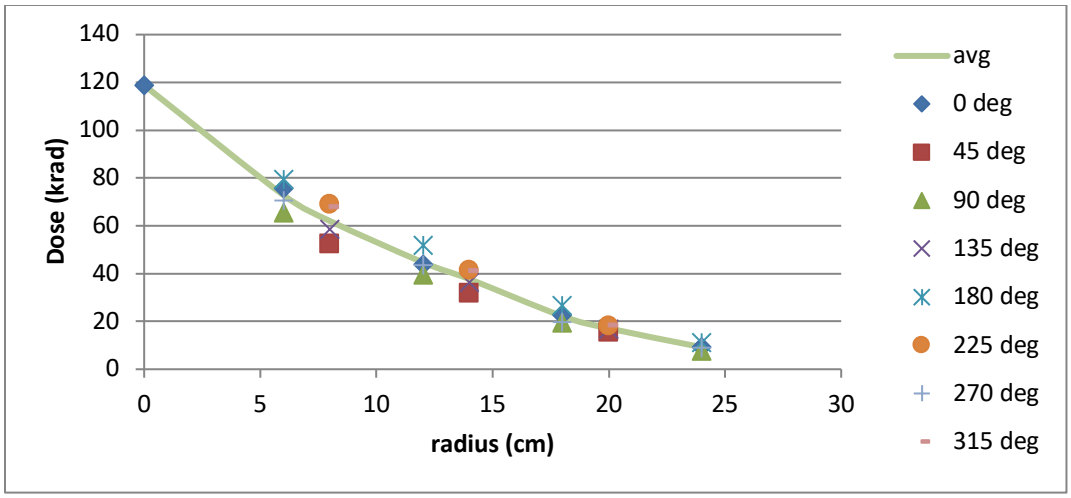

Figure 74. Shot 10436, TLD faceplate radial profile

TLD radial profile for the Shot is shown in Figure 74. The profile is clearly center-peaked. These results – electron population outside the radius of the carbon plug, but the faceplate TLD profile peaked in the center – are consistent with the MCNP Line B simulation above, with the electron impact angle on the converter at 45°.

The question can be raised then, if the electrons do not pinch, what is the source of the damage on the converter that the graphite was originally installed in place to mitigate? A counter-argument can be made that there is a difference between electron energies needed to create dose, and electron energies sufficient to cause material damage to the converter package. The latter can be less than the former. There is some experimental evidence from HERMES that supports this hypothesis. In November 2017, a series of three HERMES Standard Mode shots was taken where the graphite plug was removed and replaced with a much smaller diameter (~ 3 inches) circular disc made of tungsten (10536 – 10538). After the three shots were taken, the converter region was inspected. The tungsten disc was observed to be heavily damaged, reinforcing the notion that the graphite plug has protective benefits for the converter package. But while the resulting TLD radial profile was very similar to a graphite plug shot, the PINB signal from the middle of the three shots (10537) exhibited a very unusual waveshape, shown in Figure 75. Instead of the usual ~ monotonically increasing-then-decreasing shape, the PINB signal is characterized by a sizable secondary lobe, which begins at about the halfway mark on the usual fall, and spikes to almost as high as the main peak. Given the highly unusual nature of this waveshape (almost unique in that regard), one conclusion that can be made is that this is the signature of the electron strike that damaged the tungsten. Tungsten, being of equivalent high-Z material as tantalum, would be a source of copious photons if struck by the HERMES electron beam. Matching the timing of the secondary lobe against the voltage and current waveforms, one can conclude that the strike to the tungsten occurs when the voltage pulse has declined to an estimated 9 – 10 MV. But recall that the TLD radial profile looks much the same as a normal shot with the graphite plug in place. Hence the overall conclusion: the damage to the tungsten disc occurred at an estimated voltage that is clearly sufficient enough to cause significant material damage, yet the strike itself does not appear to significantly affect the TLD dose levels. This could occur late in the pulse, as evidenced by the PINB signal in Figure 75.

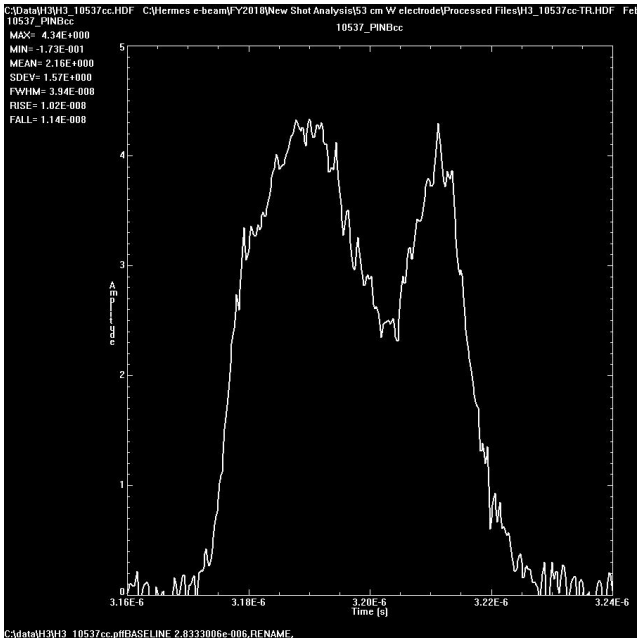

Figure 75. PINB signal from Shot 10537

The transition from non-centered to centered peak on HERMES shots can be explained thus: some process, like increased beam power liberating more ions from the converter, results in an increase to the electron angle(s) on the converter. This in turn leads to an electron beam that pinches down to the axis. However, this pinch may occur late in time, after the radiation pulse is substantially over. Also, the change in electron angle must occur at a distance fairly close to the converter location, else the physical position of the electrons would migrate closer to the axis and could impact the graphite plug. The MCNP simulations, and the x-ray pinhole camera data, clearly indicate that the electron beam itself, at least through the radiation-producing part of the power pulse, does *not* impact the graphite plug.

APPENDIX 2: PROCEDURE TO USE XDAMP TO CABLE-COMPENSATE HERMES SIGNALS WHICH ARE NOT ALREADY CABLE-COMPENSATED

This procedure requires that one possesses the hdf file **hermesuniversalcompensator.hdf**.

Obtain the waveform to be compensated from the STL site. Go to the directory for the shot number of interest. It will contain a subdirectory **xxxxx_ascii**, where xxxxx is the shot number. This directory contains **.csv** files for each of the waveforms. Load the .csv files of interest onto your computer.

The format of these files is

Waveform_name
Pairs of time,value
Here is an example.
XMB1090
2.243000e-006, -981.3382
2.243200e-006, -13.79696
2.243400e-006, 10551.75
2.243600e-006, 6588.704

However, the format of the .csv files for XDAMP has to be as follows
{space},waveform_name
s,A
pairs of time,value

For example, the first few lines of the XDAMP-readable .csv file read
,XMB1090
s,A
2.243000e-006, -3846.059
2.243200e-006, 7721.891
2.243400e-006, 4347.641
2.243600e-006, -3756.928
2.243800e-006, 292.173

Open the file in Notepad (not in Excel), add the "{space}," before the waveform name, add the second line "s,A" and then save it.

Now open XDAMP. In Options, set the file filter to *.csv and the file type to EXCEL. Open the edited .csv file, then change the file filter to *.hdf and the file type to GUIDAS. Now append the file hermesuniversalcompensator.hdf.

Before cable compensating the waveform, dedroop it if necessary. To dedroop a waveform, select the waveform to be dedrooped (can be multiple waveforms), hit the "special" button, then hit the "DeDroop" button on the dropdown menu. When it asks to input the e-folding time, enter "275E-9" (for a 275 ns dedroop factor) and push the done button. The selected waveform will be overwritten, so if you want to save the original you need to make a copy of the waveform with a different name.

To cable compensate a waveform, select the waveform to be compensated (single waveform only), hit the "enter" button on the XDAMP screen, select the compensator waveform, hit the "special" button on the XDAMP screen, then hit the "Cable Compensate" button on the drop-down menu. This will compensate

the selected waveform, and overwrite it. The selected waveform will be overwritten, so if you want to save the original you need to make a copy of the waveform with a different name.

DISTRIBUTION

2 Dr. Paul F. Ottinger
4899 Montrose Blvd Apt 1112
Houston, TX 77006

2 Dr. Bruce V. Weber
4899 Montrose Blvd Apt 1112
Houston, TX 77006

2 Russell Durrer
56 Fox Place
Pagosa Springs, CO 81147

2	MS1106	Andrew Biller	Org. 1342
2	MS1106	Sean K. Coffey	Org. 1342
2	MS1106	Theodore C. Grabowski	Org. 1342
1	MS1106	Benjamin M. Hughes	Org. 1342
2	MS1106	Nathan R. Joseph	Org. 1342
4	MS1106	Debra S. Kirschner	Org. 1342
2	MS1106	John A. Lott	Org. 1342
4	MS1106	Brent A. Melville	Org. 1342
2	MS1106	Robert A. Natal	Org. 1342
2	MS1106	Israel Owens	Org. 1342
1	MS1106	Andrew W. Shay	Org. 1342
2	MS1106	Joe G. Stewart	Org. 1342
1	MS1106	Gary D. Tilley	Org. 1342
1	MS1106	Cameron K. Tunell	Org. 1342
4	MS1152	Keith Cartwright	Org. 1352
2	MS1152	Timothy D. Pointon	Org. 1352
4	MS1167	Bryan V. Oliver	Org. 1340
10	MS1182	Timothy Renk	Org. 5445
2	MS1182	Ronald J. Kaye	Org. 5445
1	MS0899	Technical Library	9536 (electronic copy)


Sandia National Laboratories